ESD-TR-70-150

Technical Report 480

Magnetic Moment Versus Temperature Curves of Ferrimagnetic Garnet Materials

G. F. Dionne

9 September 1970

Prepared for the Office of the Chief of Research and Development,
Department of the Army,
under Electronic Systems Division Contract AF 19(628)-5167 by

Lincoln Laboratory

MASSACHUSETTS INSTITUTE OF TECHNOLOGY

Lexington, Massachusetts

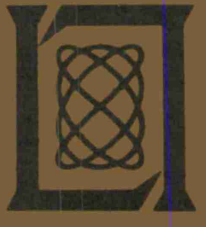

MASSACHUSETTS INSTITUTE OF TECHNOLOGY

LINCOLN LABORATORY

MAGNETIC MOMENT VERSUS TEMPERATURE CURVES OF FERRIMAGNETIC GARNET MATERIALS

G. F. DIONNE

Group 34

TECHNICAL REPORT 480

9 SEPTEMBER 1970

LEXINGTON MASSACHUSETTS

The work reported in this document was performed at Lincoln Laboratory, a center for research operated by Massachusetts Institute of Technology. The work is sponsored by the Office of the Chief of Research and Development, Department of the Army; it is supported by the Advanced Ballistic Missile Defense Agency under Air Force Contract AF 19(628)-5167.

ABSTRACT

The molecular field coefficients employed in the Néel theory of ferrimagnetism have been determined as functions of the levels of diamagnetic ion substitution in the garnet family $\{Y_zGd_{3-z}\}$ $[R_xFe_{2-x}]$ (Q_yFe_{3-y}) O_{12}, where R and Q represent diamagnetic octahedral and tetrahedral substitutions, respectively. The coefficients may be listed as

$$N_{dd} = -30.4\ (1 - 0.43x)$$

$$N_{aa} = -65.0\ (1 - 0.42y)$$

$$N_{cc} = 0$$

$$N_{ad} = 97.0\ (1 - 0.125x - 0.127y)$$

$$N_{cd} = 6.0$$

$$N_{ac} = -3.44 \text{ moles/cm}^3 \quad .$$

With these coefficients the magnetic moment versus temperature curves of compositions ranging from $0 \leqslant x \leqslant 0.70$, $0 \leqslant y \leqslant 1.95$, and $0.40 \leqslant z \leqslant 1.00$ were computed and are presented in this report.

Accepted for the Air Force
Joseph R. Waterman, Lt. Col., USAF
Chief, Lincoln Laboratory Project Office

CONTENTS

MAGNETIC MOMENT VERSUS TEMPERATURE CURVES OF FERRIMAGNETIC GARNET MATERIALS

I. INTRODUCTION

The phenomenon of ferrimagnetism has been the subject of extensive investigation since its discovery. From a phenomenological standpoint, the molecular field theory of Néel has proven to be extremely successful in explaining many of the basic properties of ferrimagnetic systems.[1] The essence of the simplest model consists of two alternating sublattices of unequal and antiparallel moments, with three molecular field coefficients employed to describe the exchange field effects: one ferromagnetic coefficient for each sublattice and a third for the antiferromagnetic interaction between the sublattices. Through proper use of Brillouin functions together with the correct values of the coefficients, it has been demonstrated that magnetization-temperature curves may be accurately reproduced. Conversely, experimental curves of this type may be used to determine the molecular field coefficients, as was demonstrated by Anderson using a trial-and-error fit for yttrium-iron garnet.[2]

In many cases, the coefficients have been determined from magnetic susceptibility measurements above the Curie temperature. Measurements of this type were reported by Pauthenet[3] and Aléonard[4] for a variety of iron garnets. A third method involving an analytical technique was demonstrated by Rado and Folen for magnesium and lithuim ferrite.[5] In each of these cases, the material may be considered as an ideal Néel ferrimagnet (i.e., no sublattice canting) since the magnetic moments at cryogenic temperatures approach their theoretical values.

When Fe^{3+} ions are replaced by diamagnetic substitutes, there is considerable experimental evidence that sublattice canting or some equivalent effect begins to take place. In a model developed by Gilleo,[6] departures from the Néel model were explained by considering that ions became paramagnetic centers when interacting with less than three nearest-neighbor cations of different coordination. For small substitutions, this model proved reasonably satisfactory but broke down quickly at higher levels.

In subsequent work, Geller and his colleagues[7] performed extensive magnetization measurements on substituted yttrium-iron garnets at cryogenic temperatures and concluded that the canting originally proposed by Yafet and Kittel[8] does occur and in a peculiar manner. When substitutions are made into one sublattice, random canting takes place in the opposite one. As the substitution level is increased, the opposite sublattice gradually reaches an antiferromagnetic state. These results led to the concept of competing ferrimagnetic and antiferromagnetic solvents. For small substitutions, the ferrimagnetic solvent dominates the antiferromagnetic solvent; after a threshold is attained at some higher level of substitution, the reverse becomes true, with the result that an abrupt change in the degree of canting is observed.

In the work to be reported here, the molecular field coefficients of several yttrium-iron garnet compositions were determined from the experimental magnetization-temperature curves reported by Gilleo and Geller.[9] The results reveal unexpected linear relationships between the coefficients and levels of substitution and strongly suggest that canting is directly related to the changes in the field constants. As a result, an attempt is made to establish a transition between the ideal ferrimagnet of Néel and the canted sublattice version discussed by Geller, as the amount of diamagnetic substitution is increased from zero to the critical regions where antiferromagnetism becomes dominant. Within the ferrimagnetic region of compositions, it should now be possible to compute with good accuracy the magnetic moment-temperature curves of yttrium-iron garnet with combinations of both octahedral and tetrahedral substitutions.

II. THEORETICAL CONSIDERATIONS

A. Néel Theory of Ferrimagnetism

According to the Néel model of ferrimagnetism, the temperature dependence of the magnetic moment per mole of each sublattice may be represented by Brillouin functions

$$M_i(T) = M_i(0)\, B_{S_i}(x) \quad , \tag{1}$$

where the subscript i refers to the particular sublattice. For the general case of the garnet structure, three sublattices must be considered: the tetrahedral (d), the octahedral (a), and the dodecahedral (c), with the last containing rare-earth ions. In this work, the discussion will be confined to the two-sublattice case, i.e., d- and a-sites containing Fe^{3+} magnetic ions. The three-sublattice case is outlined in Appendix A.

For this case, the magnetic moment per mole is given by

$$M(T) = M_d(T) - M_a(T) \quad , \tag{2}$$

where

$$M_d(T) = M_d(0)\, B_{S_d}(x_d)$$

$$M_a(T) = M_a(0)\, B_{S_a}(x_a) \quad .$$

The Brillouin functions are expressed as

$$B_{S_d} = \left(\frac{2S_d + 1}{2S_d}\right) \coth \left(\frac{2S_d + 1}{2S_d}\right) x_d - \frac{1}{2S_d} \coth \left(\frac{1}{2S_d}\right) x_d$$

$$B_{S_a} = \left(\frac{2S_a + 1}{2S_a}\right) \coth \left(\frac{2S_a + 1}{2S_a}\right) x_a - \frac{1}{2S_a} \coth \left(\frac{1}{2S_a}\right) x_a \quad , \tag{3}$$

with

$$x_d = \frac{S_d g \mu_B}{kT} (N_{dd} M_d + N_{da} M_a)$$

$$x_a = \frac{S_a g \mu_B}{kT} (N_{ad} M_d + N_{aa} M_a) \quad . \tag{4}$$

In Eq. (4), N_{dd}, N_{aa}, and $N_{da} = N_{ad}$ are the molecular field coefficients, S_d and S_a are the spin quantum numbers (5/2 for the high-spin state) of the Fe^{3+} ions occupying the d- and a-sites, respectively, g is the spectroscopic splitting factor (= 2.0), μ_B is the Bohr magneton, and k is the Boltzmann constant.

At T = 0°K, the magnetic moments per mole for each sublattice are given by

$$M_d(0) = 3gS_d\mu_B N(1 - k_d)$$

$$M_a(0) = 2gS_a\mu_B N(1 - k_a) \quad , \tag{5}$$

where k_d and k_a represent the fractions of diamagnetic ions substituted for Fe^{3+} ions in the respective sublattice and N is Avogadro's number. The factors 3 and 2 appearing in Eq. (5) represent the relative numbers of d- and a-sites in the garnet formula unit. The above theory represents the essence of the Néel model, which is based on antiparallelism between the moments of the two sublattices. As indicated in Figs. 1 and 2, which are replots of Geller's data,[7] there are discrepancies between the experimental results and the Néel model. For $k_d \leqslant 0.65$ and $k_a \leqslant 0.35$, the differences are minor. However, above these values, the departures become enormous and may be explained only by assuming significant changes in the spin arrangments of at least one of the sublattices.

According to Geller, these departures from the Néel model are caused by random canting within the individual sublattices. Initially, the canting is relatively small, but increases quickly as the transition points are reached and the antiferromagnetic tendencies dominate. In the work to be described, it will be necessary to compute $M_d(0)$ and $M_a(0)$ below the transition points, and it is clear from Figs. 1 and 2 that the Néel model given by Eq. (5) will not be adequate. As mentioned earlier, Gilleo[6] has attempted to solve this problem by means of a statistical model. Although his results provided better agreement with the data, the fit was not satisfactory over the entire range of interest in this work, i.e., $k_d \leqslant 0.65$ and $k_a \leqslant 0.35$. In order to reproduce from theory the experimental values of the sublattice moments at T = 0°K the following modifications to Eq. (5) were determined empirically as the only convenient recourse:

$$M_d(0) = 3gS_d\mu_B N(1 - k_d)\,(1 - 0.1\,k_a)$$

$$M_a(0) = 2gS_a\mu_B N(1 - k_a)\,(1 - k_d^{5.4}) \tag{6}$$

There is no obvious explanation of why a linear factor appears to work in one case while an exponential will suffice in the other. Clearly, both factors are but approximations to a more general theory yet to be devised. As will be demonstrated later, the answer is probably related to the initial magnitudes of the intra-sublattice molecular field coefficients or the relative strengths of the d and a sublattice exchange energies.

Before this section is completed, it should be mentioned that all of the magnetic moments in the figures to follow are expressed in Bohr magnetons per formula unit, or

$$\eta_B = \frac{M}{\mu_B N} \quad , \tag{7}$$

where pertinent. All other quantities involved were expressed in units of the cgs system.

B. Theoretical Model

The basic approach to this problem was the trial-and-error determination of the correct combination of N_{dd}, N_{aa}, and N_{ad} required to fit a given set of data. For pure $Y_3Fe_5O_{12}$, a set of coefficients had already been furnished by Anderson.[2] Since the molecular field coefficient is directly related to the strength of an exchange field, it is not possible to justify increases in magnitude with diamagnetic substitutions. As a result, only reductions in the magnitudes of the coefficients were considered as physically realistic. It also became apparent that when substitutions were confined to one sublattice, it was not possible to obtain a good fit with experiment by reducing the magnitudes of both N_{dd} and N_{aa} simultaneously, because excessive reductions in the Curie temperature led to increases in N_{ad}. From these observations, the following conclusions were drawn: (1) to a first approximation, substitutions in the d sublattice cause reductions in $|N_{aa}|$ without changing $|N_{dd}|$, and vice versa, and (2) $|N_{ad}|$ decreases regardless of the site distribution of the diamagnetic ions.

To place this reasoning on a firmer physical basis, consider an ion of moment $\vec{\mu}_i$ in a molecular field $\vec{H}_i$ (Ref. 10). The interaction energy may be expressed as

$$E = -\vec{\mu}_i \cdot \vec{H}_i \tag{8}$$

or

$$E = -g_i \mu_B \vec{S}_i \cdot \sum_j N_{ij} \vec{M}_j \quad . \tag{9}$$

Since this energy is equivalent to the sum of the exchange interactions with its near neighbors,

$$E = -2 \sum_j z_{ij} J_{ij} \vec{S}_i \cdot \vec{S}_j \quad , \tag{10}$$

where z_{ij} represents the number of nearest neighbors on the j^{th} sublattice that interact with the i^{th} ion and J_{ij} is the exchange constant. Since

$$M_j = n_j g_j \mu_B S_j \quad , \tag{11}$$

where n_j is the number of ions per mole in j^{th} sublattice, the molecular field constant may be found by combining Eqs. (9), (10), and (11):

$$N_{ij} = \left(\frac{z_{ij}}{n_j}\right) 2 \frac{J_{ij}}{g_i g_j \mu_B^2} \quad . \tag{12}$$

In cases where random substitutions are considered, (z_{ij}/n_j) is unaffected (assuming z_{ij} is treated as an average) and the only variable is J_{ij}, which must also be considered as an average. Therefore, the molecular field coefficients should be directly proportional to the average exchange constants as

$$\begin{aligned} N_{dd} &\propto \langle J_{dd} \rangle \\ N_{aa} &\propto \langle J_{aa} \rangle \\ N_{ad} &\propto \langle J_{ad} \rangle \end{aligned} \tag{13}$$

When a magnetic ion is removed from the d sublattice, as sketched in Fig. 3, all of the nearest-neighbor a cations experience the loss of a fraction of their superexchange interactions through canting. In other words, the local J_{aa} and J_{ad} are weakened to J'_{aa}, J''_{aa}, and J'_{ad}, while to a first approximation, the d sublattice is affected only insofar as it suffers the loss of moment associated with the missing ion.

Both sublattices consequently suffer reductions in molecular field strengths, one through reduced exchange and the other through a loss in total magnetic moment. However, as indicated by Eq. (13), only N_{aa} and N_{ad} will change because of lower values of $\langle J_{aa} \rangle$ and $\langle J_{ad} \rangle$. Since $\langle J_{dd} \rangle$ is unaffected, N_{dd} remains the same. These general arguments also apply to the case where an a-site magnetic ion is removed, with the result that N_{aa} will be unaffected.

The relationship of this model to that of Geller is almost axiomatic. If the molecular fields are considered as bases for the parallelism of the sublattices, it is evident that any tendency toward canting would of necessity depend on reductions in the magnitudes of these coefficients. Since Geller has pointed out the tendency toward antiferromagnetism at higher substitutions, it seems likely that this trend should initially be manifested by changes in the values of N_{dd}, N_{aa}, and N_{ad}. This subject will be discussed more fully in a later section.

III. DETERMINATION OF MOLECULAR FIELD COEFFICIENTS

In Figs. 4, 5, 8, and 9, the "best-fit" magnetic moment versus temperature curves of several compositions are plotted together with the experimental points determined by Gilleo and Geller.[9] For purposes of comparison, the dashed-line curves computed by using the molecular field coefficients of pure $Y_3Fe_5O_{12}$ (see Table I) are also included. The sequence employed in this

TABLE I

MOLECULAR FIELD COEFFICIENTS OF SUBSTITUTED $Y_3Fe_5O_{12}$

Composition	k_d	k_a	N_{dd} moles/cm^3	N_{aa} moles/cm^3	N_{ad} moles/cm^3
$Y_3Fe_5O_{12}$	0	0	−30.4	−65.0	97.0
$Y_3Sc_{0.25}Fe_{4.75}O_{12}$	0	0.125	−27.0	−65.0	94.0
$Y_3In_{0.50}Fe_{4.50}O_{12}$	0	0.25	−24.0	−65.0	91.0
$Y_3Ga_{0.25}Fe_{4.75}O_{12}$	0.075	0.0125	−30.1	−59.0	94.0
$Y_3Ga_{0.75}Fe_{4.25}O_{12}$	0.22	0.04	−29.4	−47.0	88.0
$Y_3Al_{0.33}Fe_{4.67}O_{12}$	0.105	0.007	−30.2	−56.0	93.0
$Y_3Al_{1.0}Fe_{4.0}O_{12}$	0.28	0.07	−28.6	−42.0	85.0

work was as follows: from pure octahedral (a-site) substitutions of Sc^{3+} and In^{3+} shown in Figs. 4 and 5, the curves were fitted by reducing $|N_{dd}|$ and $|N_{ad}|$. The results were then plotted as functions of k_a as in Figs. 6 and 7, where it was found that linear relations exist in both cases. From the slopes of these straight-line curves,

$$N_{dd} = -30.4 + 26.4 k_a$$

$$N_{ad} = 97.0 - 24.0 k_a \quad (\text{for } k_d = 0) \quad . \tag{14}$$

With these expressions it was then possible to fit the results for the Ga^{3+} and Al^{3+} substituted compositions shown in Figs. 8 and 9. After determining the values of k_a and k_d from the moments at T = 0°K, the values of N_{dd} for all four of these compounds were calculated from Eq. (14). These values were then used in determining the proper theoretical fits, which were obtained this time by varying N_{aa} and N_{ad}. The results for the molecular field coefficients of all compositions studied are listed in Table I.

As before, the values of N_{aa} were found to have a linear dependence on k_d, as indicated by the appropriate curve in Fig. 6. In the case of N_{ad}, the results from Fig. 7 were employed with $(N_{ad} + 24 k_a)$ plotted as a function of k_d in Fig. 10 in order to reveal the linearity and determine the correct slope. The results may thus be expressed as

$$N_{dd} = -30.4 (1 - 0.87 k_a)$$

$$N_{aa} = -65.0 (1 - 1.26 k_d)$$

$$N_{ad} = 97.0 (1 - 0.25 k_a - 0.38 k_d) \quad , \tag{15}$$

subject to the limitations of $k_a \leqslant 0.35$ and $k_d \leqslant 0.65$.

Since $k_d = y/3$ and $k_a = x/2$, where y and x are the numbers of substituted diamagnetic ions per formula unit occupying d- and a-sites respectively, Eq. (15) may be written as

$$N_{dd} = -30.4 (1 - 0.43x)$$

$$N_{aa} = -65.0 (1 - 0.42y)$$

$$N_{ad} = 97.0 (1 - 0.125x - 0.127y) \tag{16}$$

for $x \leqslant 0.70$ and $y \leqslant 1.95$. From Eq. (16) it may be readily deduced that

$$\left|\frac{\Delta N_{ad}}{N^{\circ}_{ad}}\right| \simeq +0.3 \left(\left|\frac{\Delta N_{dd}}{N^{\circ}_{dd}}\right| + \left|\frac{\Delta N_{aa}}{N^{\circ}_{aa}}\right| \right) \quad , \tag{17}$$

where $N^{\circ}_{dd} = -30.4$, $N^{\circ}_{aa} = -65.0$, and $N^{\circ}_{ad} = 97.0$.

It is indeed curious that the numerical coefficients of x and y in Eq. (16) are so similar. Although there is no explanation to be offered at this time, the following observation will be made. When a d-site Fe^{3+} ion is replaced, four nearest-neighbor a-site Fe^{3+} ions are directly affected. However, when the reverse occurs, six nearest neighbors are involved, an increase of fifty percent. Thus, the ratio of the number of sites affected to the total number of sites within a given sublattice is effectively the same in both cases. Therefore, it must follow that the contributions to the percentage decrease in the coefficient from each affected site must also be the same in both cases, in order to produce the above relations for N_{dd} and N_{aa}. As a direct result of this, it should not be surprising to find the symmetry expressed in Eq. (17).

With the results given by Eq. (15), it should now be possible to compute the magnetic moment-temperature curve for any substitution below the antiferromagnetic transition points. In Figs. 11 and 12, normalized curves are plotted for pure tetrahedral and octahedral substitutions respectively, and reveal the extent to which the shape of the curve may vary as the molecular field coefficients change. As a test for systems containing diamagnetic ions in both sites, the experimental results for $\{Y_3\}\,[Mg_xFe_{2-x}]\,(Fe_{3-x}Si_x)\,O_{12}$ (Ref. 7) are compared with theory in Fig. 13. The agreement is excellent up to the levels of substitution indicated, without any indication of a possible breakdown at higher concentrations.

IV. SUBLATTICE CANTING

In the development of Eq. (6), it was stated that random canting of the sublattice opposite to that in which substitutions are made was concluded from the extensive experimental work of Geller.[7] Since canting effects were observed more readily in the tetrahedral sublattice, it was decided that its tendency towards antiferromagnetic alignment was greater than for the octahedral case. In this sense, d-d interactions were considered to be stronger than a-a interactions. In this present work, the pseudo-ferromagnetism of the individual sublattices is chosen as the basis for discussion because of its obvious relation to the sign and magnitudes of N_{dd} and N_{aa}. From this standpoint, the tetrahedral sublattice is considered to have the weaker ferromagnetic interaction because $|N_{dd}| < |N_{aa}|$.

In the model depicted in Fig. 3, the nearest-neighbor magnetic moments of the sublattice are shown as canted when a particular d ion is removed. If indeed this occurs, it would be surprising to find that a reduction in $|N_{aa}|$ did not also occur. In Fig. 14, the percentage change from canting in the Bohr magnetons per formula unit at T = 0°K, $\Delta\eta_B^i/\eta_B^i$, is plotted as a function of the sublattice molecular-field coefficient N_{ii}. The results point to a close relationship between these two variables, as both curves approach the same linear function just prior to the antiferromagnetic transition which sets in at $N_{ii} \simeq -20$ moles/cm^3,

$$\frac{\Delta\eta_B^i}{\eta_B^i} = -(3.75N_{ii} + 11.4) \times 10^{-3} \quad . \tag{18}$$

As suggested by Geller, the canting effects theoretically should be expected immediately upon diamagnetic substitutions into either sublattice. For the d sublattice, the change is immediately detectable, as seen by Fig. 2, because of its relatively weak molecular field coefficient $N_{dd} = -30.4$. With $N_{aa} = -65.0$, a significant amount of tetrahedral substitution is required before the coefficient drops to the point where departures from the Néel model are detected.

V. CONCLUSIONS

In the foregoing sections, a description of the method used in determining the molecular field coefficients of several substituted yttrium-iron garnets was presented. The coefficients were found by fitting the Néel theory to experimental magnetic moment versus temperature curves below the antiferromagnetic transition substitution levels of $k_d \leqslant 0.65$ and $k_a \leqslant 0.35$.

In general, it was found that peculiar linear relations exist between the coefficients N_{dd}, N_{aa}, and N_{ad} and the fractions of sublattice substitution k_d and k_a. For substitutions in one sublattice, the coefficient of the opposite sublattice is reduced in magnitude while its own coefficient remains unchanged; for substitutions in either sublattice, the inter-sublattice coefficient

N_{ad} is reduced. By comparing the magnitudes of the coefficients with the changes in sublattice moment from canting, it was found that at these lower levels of substitution, the amount of canting in a given sublattice appears to be directly related to a change in its molecular field coefficient. This result provides a tie between the Néel theory and the random canting concepts of Geller and serves to confirm that canting begins to set in immediately upon substitution.

Since $|N_{dd}| < |N_{aa}|$ initially, canting would be expected to occur earlier in the tetrahedral sublattice, in accord with Geller's observations. This result also conforms with the notion that the d sublattice has a stronger antiferromagnetic interaction, because the weaker $|N_{dd}|$ coefficient refers to the strength of ferromagnetic interaction. If it is weaker ferromagnetically, it must follow that it is stronger antiferromagnetically.

Finally, because it is possible to express the coefficients as analytical functions of the amounts of substitutions, it appears likely that for ions of the valence states involved in this study, magnetic moment-temperature curves may be computed readily for any level of substitution below the antiferromagnetic transitions.[11] In situations where the levels of substitution in both sublattices approach their limits, some question of applicability still remains. However, the results shown in Fig. 13 suggest that there is good reason for optimism on this point.

ACKNOWLEDGMENT

The author is greatly indebted to Janet Reid and Susan Rajunas for the computer programming necessary to carry out these investigations.

REFERENCES

1. L. Néel, Ann. Physique (12) 3, 137 (1948).
2. E.E. Anderson, Phys. Rev. 134, A1581 (1964).
3. R. Pauthenet, Doctoral Thesis, University of Grenoble (1957).
4. R. Aléonard, J. Phys. Chem. Solids 15, 167 (1960).
5. G.T. Rado and V.J. Folen, J. Appl. Phys. 31, 62 (1960).
6. M.A. Gilleo, J. Phys. Chem. Solids 13, 33 (1960).
7. S. Geller, H.J. Williams, G.P. Espinosa, and R.C. Sherwood, Bell System Tech. J. 43, 565 (1964).
8. Y. Yafet and C. Kittel, Phys. Rev. 87, 290 (1952).
9. M.A. Gilleo and S. Geller, Phys. Rev. 110, 73 (1958).
10. J.B. Goodenough, Magnetism and the Chemical Bond (Interscience Publishers John Wiley & Sons, New York, 1963) p. 118.
11. S. Geller, H.J. Williams, R.C. Sherwood, and G.P. Espinosa, J. Appl. Phys. 36, 88 (1965).
12. A. Vassiliev, J. Nicolas, and M. Hildebrandt, C.R. Acad. Sci. (Paris) 252, 2529 (1961).
13. G.R. Harrison and L.R. Hodges, Jr., J. Appl. Phys. 33, 1375 S (1962).
14. E.E. Anderson, J.R. Cunningham, Jr., and G.E. McDuffie, Phys. Rev. 116, 624 (1959).

APPENDIX A

For the three sublattice case, the Néel theory must be augmented as follows:

$$M = M_a + M_c - M_d \quad , \tag{A-1}$$

where

$$M_i(T) = M_i(0)\, B_{s_i}(x_i)$$

$$x_d = \frac{S_d g \mu_B}{kT} (N_{dd}M_d + N_{da}M_a + N_{dc}M_c)$$

$$x_a = \frac{S_a g \mu_B}{kT} (N_{ad}M_d + N_{aa}M_a + N_{ac}M_c) \tag{A-2}$$

$$x_c = \frac{S_c g \mu_B}{kT} (N_{cd}M_d + N_{ca}M_a + N_{cc}M_c)$$

with $N_{da} = N_{ad}$, $N_{dc} = N_{cd}$ and $N_{ac} = N_{ca}$.

At T = 0°K, the magnetic moments per formula unit are given by

$$M_d(0) = 3gS_d\mu_B N(1 - k_d)\,(1 - 0.1\,k_a)$$

$$M_a(0) = 2gS_a\mu_B N(1 - k_a)\,(1 - k_d^{5.4}) \tag{A-3}$$

$$M_c(0) = 3gS_c\mu_B N(1 - k_c) \quad ,$$

where k_c is the fraction of Y^{3+} ions in c-sites and $S_c = 7/2$ for Gd^{3+}.

For Gd^{3+} substitutions into the c-sublattice, the Néel model is used without modification because the effects of canting both in the sublattice itself and in the other sublattices are judged to be negligible at the levels of substitution involved. This conclusion is based on inspection of the work of Geller et al.,[11] who reported data on the garnet families containing Gd^{3+} ions. To a first approximation, the molecular field coefficients of the c-sublattice are considered to be independent of composition.

The molecular field coefficients may be listed as follows:

$$N_{dd} = -30.4\,(1 - 0.87\,k_a) \qquad N_{ad} = 97.0\,(1 - 0.25\,k_a - 0.38\,k_d)$$

$$N_{aa} = -65.0\,(1 - 1.26\,k_d) \qquad N_{cd} = 6.0$$

$$N_{cc} = 0 \qquad N_{ac} = -3.44\ \text{moles/cm}^3 \quad . \tag{A-4}$$

In Figs. 15, 16, and 17, comparisons between theory and experiment are presented to illustrate the accuracy of the computed curves. Those discrepancies which may not be accounted for by experimental error are probably the result of the small canting effects which have been ignored. Since the data in Fig. 17 were not corrected for porosity (which could have been as high as 5 percent), it may be assumed that the agreement could be significantly improved.

APPENDIX B
COMPUTER PROGRAM

```
C     MAIN PROGRAM FOR 3 MOMENTS-- USING SUBROUTINE MOM3 FOR CON-
C     VERGENCE.  G. DIONNE
      IMPLICIT REAL*8 (A-H,K,M,N,O-Z)
      COMMON /M1/ SD,SA,SC,MUB,K,BN,G
      COMMON /M2/ NDD,NAA,NAD,NAC,NCD,NCC
      COMMON /M3/ KD,KA,KC
      COMMON /ANS/ M,MD1,MA1,MC1,NBANS
      DIMENSION TEMP(200),NB(200),KAA(21),KDD(21),NBB(21,200),MSAVE(21),
     1KCC(5)
C     THE FOLLOWING ARRAYS ARE USED IN PLOTTING ONLY
      DIMENSION TITLE(9),YY(1700),TT(1700),LC(21)
C     T1 AND T2 ARE LABELS FOR THE X AND Y AXES
      DATA T1/'TEMP'/,T2/'NB  '/
      DATA KCC/.8,.7,.6,.5,.4/
C     THE FOLLOWING TWO LINES REFER TO ROUTINES ACCESSIBLE TO USERS OF
C     LINCOLN'S 360/67 AND PERTAIN ONLY TO THE PLOTTING
      CALL REREAD(15,80)
      CALL STOIDV(' G. DIONNE',9,0)
      SD=2.5
      SA=2.5
      SC=3.5
      MUB=9.27E-21
      K=1.38E-16
      BN=6.023E+23
      G=2.0
      NCD=6.0
      NAC=-.5734*NCD
      NCC=0.0
C     INITIAL KA VALUE
      KAA(1)=.05
C     INITIAL KD VALUE
      KDD(1)=.35
C     INCREMENT FOR KA AND KD
      DK=.01
C     INCREMENT FOR TEMPERATURE
      DT=10.
C     NUMBER OF CURVES PER PAGE (NUMBER OF KD'S USED)
      ICURVE=11
      DO 59 L=1,ICURVE
      KAA(L)=KAA(1)+(L-1)*DK
   59 KDD(L)=KDD(1)+(L-1)*DK
C     DO 218 LRR=1,5
C     KC=KCC(LRR)
      KC=1.0
      DO 100 LKA=1,6
      KA=KAA(LKA)
C     THE FOLLOWING 3 LINES ARE RELEVANT ONLY TO THE PLOTTING
      IXZ=0
      NMAX=-25.E+25
      NMIN=25.E+25
      DO 200 LKD=1,ICURVE
      KD=KDD(LKD)
      NDD=-30.4*(1.-.87*KA)
      NAA=-65.*(1.-1.26*KD)
      NAD=97.*(1.-.25*KA-.38*KD)
      TEMP(1)=0.0
      TEMP(2)=20.
      IF(KD.LT..10.OR.KA.LT..10.OR.KC.LT..10) TEMP(2)=40.
      IF(TEMP(2).EQ.40.) GO TO 21
      TEMP(29)=293.
      TEMP(35)=343.
      DO 31 L=2,28
   31 TEMP(L)=TEMP(2)+(L-2)*DT
      DO 32 L=30,34
```

```
   32 TEMP(L)=TEMP(28)+(L-29)*DT
      DO 33 L=36,72
   33 TEMP(L)=TEMP(34)+(L-35)*DT
      GO TO 22
   21 TEMP(28)=293.
      TEMP(34)=343.
      DO 34 L=2,27
   34 TEMP(L)=TEMP(2)+(L-2)*DT
      DO 35 L=29,33
   35 TEMP(L)=TEMP(27)+(L-28)*DT
      DO 36 L=35,72
   36 TEMP(L)=TEMP(33)+(L-34)*DT
   22 CALL MOM3
      M1=1.
      M2=-9999.
      DO 70 L=1,72
      T=TEMP(L)
      CALL CONTIN(T,ITER,IER)
      IF(IER.EQ.1) GO TO 150
      IF(TEMP(2).EQ.20..AND.L.EQ.29) M1=M
      IF(TEMP(2).EQ.20..AND.L.EQ.35) M2=M
      IF(TEMP(2).EQ.40..AND.L.EQ.28) M1=M
      IF(TEMP(2).EQ.40..AND.L.EQ.34) M2=M
      NBB(LKD,L)=NBANS
   70 CONTINUE
  150 IF(IER.EQ.1) LC(LKD)=L-1
      IF(IER.EQ.0) LC(LKD)=L
      MSAVE(LKD)=(M1-M2)/M1
      LE=LC(LKD)
C     THE FOLLOWING DO LOOP FORMS THE ARRAY OF ABSCISSAS FOR THE POINTS
C     TO BE PLOTTED
      DO 77 LA=1,LE
      IXZ=IXZ+1
   77 TT(IXZ)=TEMP(LA)
  200 CONTINUE
      WRITE(6,4) KC
    4 FORMAT(//' KC=',F5.2)
      WRITE(6,888)
      DO 98 LN=1,ICURVE
   98 WRITE(6,999) KA,KDD(LN),NBB(LN,1),TEMP(LC(LN)),MSAVE(LN)
  888 FORMAT(/10X,'KA',7X,'KD',7X,'NB AT TEMP=0',7X,'TEMP LIMIT',
     17X,'(M1-M2)/M1')
  999 FORMAT(8X,F5.3,4X,F5.3,8X,F8.3,10X,F8.3,7X,E12.5)
C     THE FOLLOWING DO LOOP FORMS THE ARRAY OF ORDINATES FOR THE POINTS
C     TO BE PLOTTED
      IN=0
      DO 61 LKD=1,ICURVE
      LP=LC(LKD)
      DO 61 LZ=1,LP
      IN=IN+1
      IF(LC(LKD).EQ.1) GO TO 61
      IF(NBB(LKD,LZ).GT.NMAX) NMAX=NBB(LKD,LZ)
      IF(NBB(LKD,LZ).LT.NMIN) NMIN=NBB(LKD,LZ)
   61 YY(IN)=NBB(LKD,LZ)
C     THE NEXT 6 LINES WRITE ON A 9-TRACK TAPE THE INFORMATION WHICH
C     DATAGRAPHIX'S D-4060 CONVERTS INTO FINISHED PLOTS
      WRITE(15,3) KC,KA,(KDD(LSD),LSD=1,ICURVE)
    3 FORMAT(' KC=',F5.3,' KA=',F5.3,' KD=',10(F3.2,','),F3.2)
      READ(15,39) TITLE
   39 FORMAT(9A8)
      CALL GRAPH(TT,YY,ICURVE,LC,TITLE,2)
      CALL LINEAR(0.,740.,0.,NMAX,T1,T2,2)
  100 CONTINUE
  218 CONTINUE
C     THIS CALL SIGNALS THE END OF PLOTTING
      CALL PLTND
   99 CALL EXIT
      END
```

```
C     CALCULATION OF M VS TEMP FOR GARNETS WITH GD (+03)
      SUBROUTINE MOM3
      IMPLICIT REAL*8 (A-H,K,M,N,O-Z)
      COMMON /M1/ SD,SA,SC,MUB,K,BN,G
      COMMON /M2/ NDD,NAA,NAD,NAC,NCD,NCC
      COMMON /M3/ KD,KA,KC
      COMMON /ANS/ M,MD1,MA1,MC1,NB
      P=MUB*BN
      MDO=3.*G*SD*P*(1.-KD)*(1.-.1*KA)
      MAO=2.*G*SA*P*(1.-KA)*(1.-KD**(5.4))
      MCO=3.*G*SC*P*(1.-KC)
      C1=1./(2.*SD)
      C2=(2.*SD+1.)*C1
      C3=1./(2.*SA)
      C4=(2.*SA+1.)*C3
      C5=1./(2.*SC)
      C6=(2.*SC+1.)*C5
      MD=MDO
      MA=MAO
      MC=MCO
      MD1=MDO
      MA1=MAO
      MC1=MCO
      RETURN
C*************************************************************************
      ENTRY CONTIN(T,ITER,IER)
      ITER=0
      IER=0
      IF(T.EQ.0.0) M=DABS(MD-MA-MC)
      IF(T.EQ.0.0) GO TO 55
      FR=G*MUB/(K*T)
      IX=1
    9 ITER=ITER+1
      IF(ITER.GE.300) GO TO 999
      XD=SD*FR*(NDD*MD+NAD*MA+NCD*MC)
      XA=SA*FR*(NAA*MA+NAD*MD+NAC*MC)
      XC=SC*FR*(NCC*MC+NCD*MD+NAC*MA)
      BSD=C2*DCOSH(XD*C2)/DSINH(XD*C2)-C1*DCOSH(XD*C1)/DSINH(XD*C1)
      BSA=C4*DCOSH(XA*C4)/DSINH(XA*C4)-C3*DCOSH(XA*C3)/DSINH(XA*C3)
      BSC=C6*DCOSH(XC*C6)/DSINH(XC*C6)-C5*DCOSH(XC*C5)/DSINH(XC*C5)
      MD2=MDO*BSD
      MA2=MAO*BSA
      MC2=MCO*BSC
      GO TO (13,14),IX
   13 IX=2
      MD1=MD
      MA1=MA2
      MC1=MC2
      GO TO 15
   14 IX=1
      MD1=MD2
      MA1=MA
      MC1=MC2
   15 IF(DABS(MA1-MA).LT..0001.AND.DABS(MD1-MD).LT..0001
     1.AND.DABS(MC1-MC).LT..0001) GO TO 8
      MD=MD1
      MA=MA1
      MC=MC1
      IF(MD.LT.0.0.OR.MA.LT.0.0.OR.MC.LT.0.0) GO TO 999
      GO TO 9
    8 M=DABS(MD-MA-MC)
   55 NB=M/(MUB*BN)
      GO TO 888
  999 IER=1
  888 RETURN
      END
```

APPENDIX C

By systematically varying parameters k_c, k_d and k_a, magnetic moment versus temperature curves for a wide range of diamagnetic substitutions were generated from the computer program stated in Appendix B. Within the limits established in the text, k_a was varied in steps of 0.05 between 0 and 0.35. The parameter k_d was varied between 0 and 0.50, also in steps of 0.05, except for $k_c = 1.0$ where it was extended to 0.65. Finally, the parameter k_c, which defines the relative amounts of Y^{3+} and Gd^{3+} in the dodecahedral sites, was varied between 0.4 and 1.0 in steps of 0.10. Values of k_c below 0.4 were not included because they were considered to represent compositions outside of the current range of practical interest. If desired, they may be readily calculated following the procedure outlined in the computer program.

The results of these computations are presented in Figs. 18 through 25.

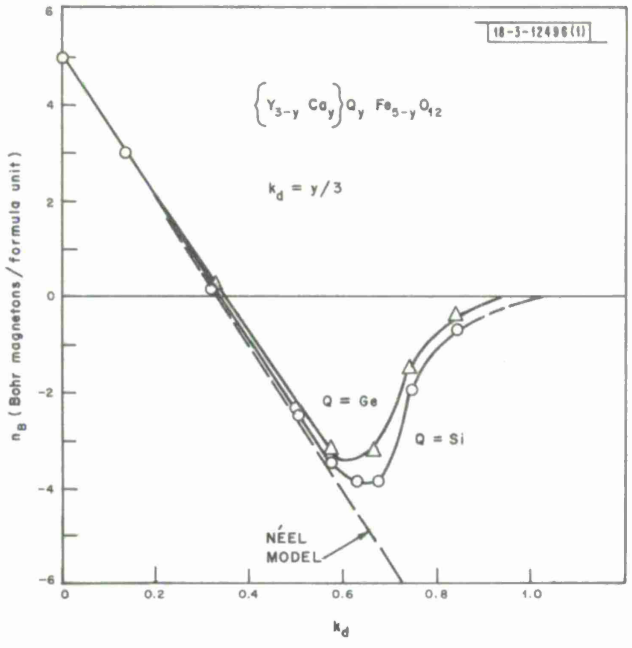

Fig. 1. Replot of Geller's magnetic moment data at T = 0°K for pure tetrahedral substitutions, indicating a departure from the Néel model. Transition to the antiferromagnetic state occurs at $k_d \simeq 0.65$.

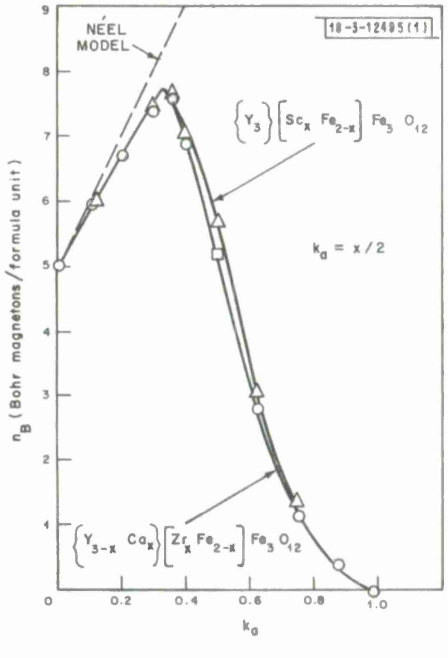

Fig. 2. Replot of Geller's magnetic moment data at T = 0°K for pure octahedral substitutions, indicating a departure from the Néel model. Transition to the antiferromagnetic state occurs at $k_a \simeq 0.35$.

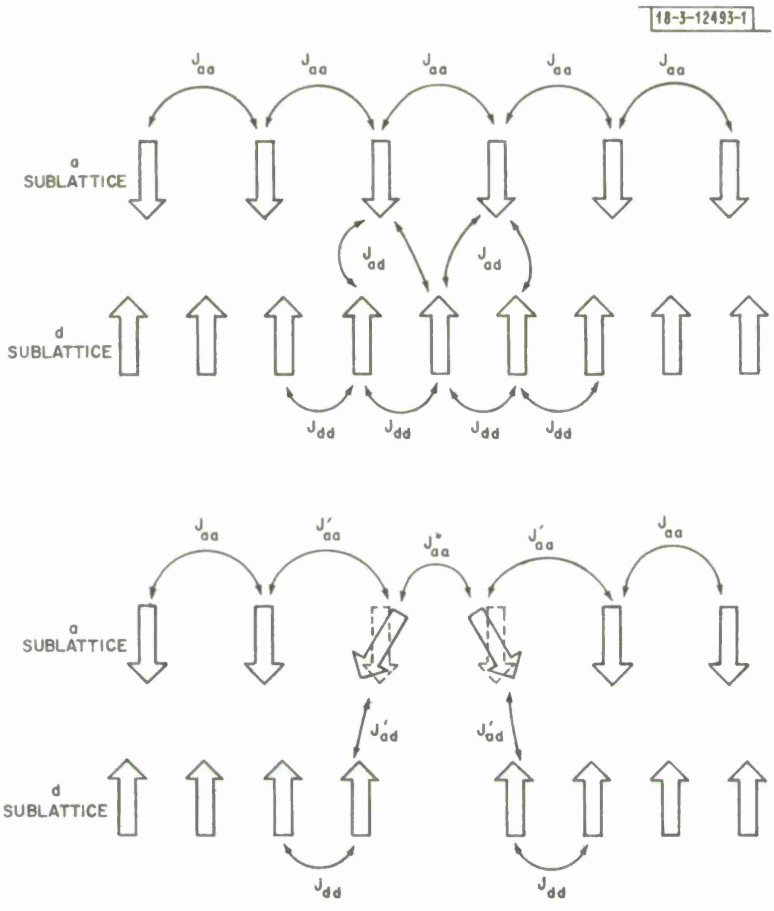

Fig. 3. Two-dimensional model of ferrimagnetic sublattices, suggesting possible effects on near-neighbor magnetic moments when a diamagnetic substitution is made in the d sublattice. Lower part indicates that canting of local octahedral site moments may occur when a magnetic ion is removed from a tetrahedral site. The argument applies equally well to tetrahedral site canting from octahedral site substitutions.

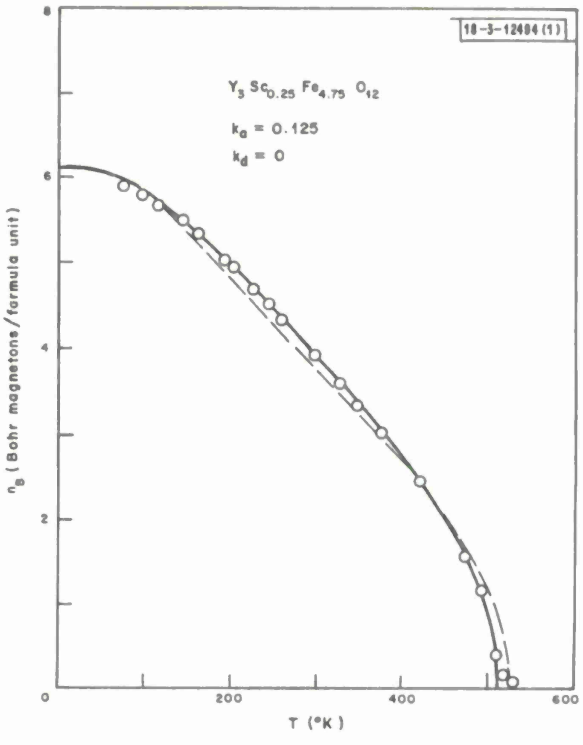

Fig. 4. Comparison of theory and experiment for magnetic moment-temperature curve of $Y_3Sc_{0.25}Fe_{4.75}O_{12}$. Dashed line represents the result calculated by using the molecular field coefficients of pure $Y_3Fe_5O_{12}$.

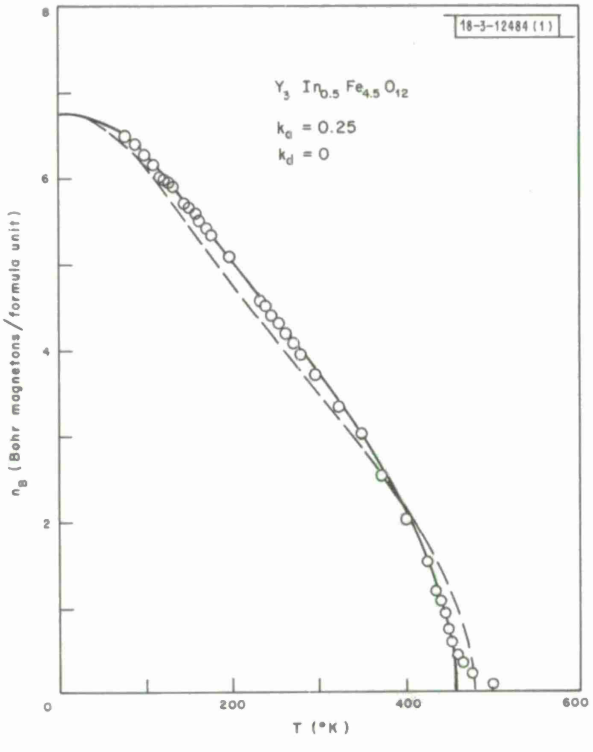

Fig. 5. Comparison of theory and experiment for magnetic moment-temperature curve of $Y_3In_{0.5}Fe_{4.5}O_{12}$. Dashed line represents the result calculated by using the molecular field coefficients of pure $Y_3Fe_5O_{12}$.

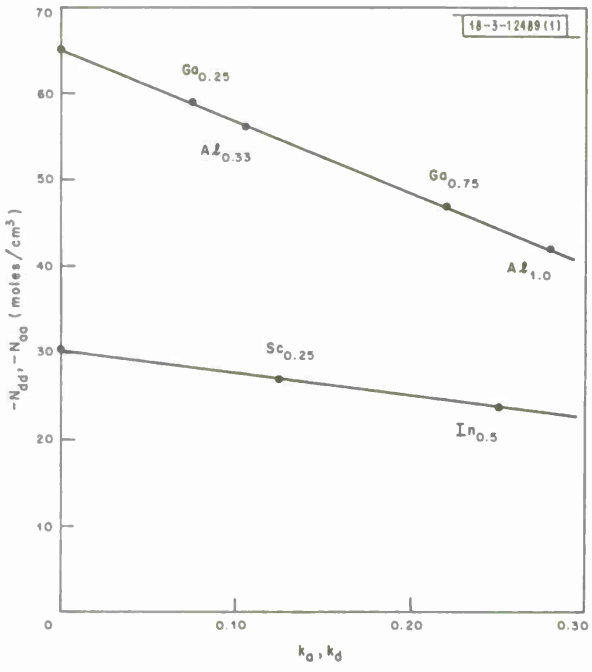

Fig. 6. Linear variations of N_{dd} and N_{aa} with k_a and k_d, respectively. Upper curve is for N_{aa}.

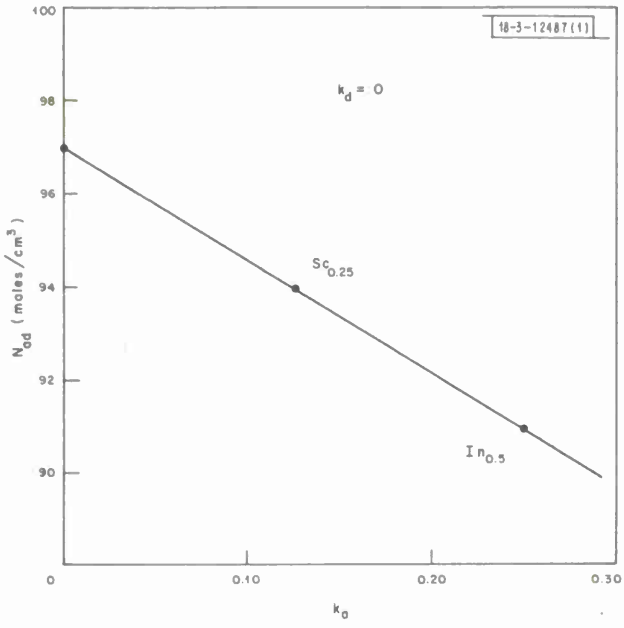

Fig. 7. Linear variation of N_{ad} with k_a ($k_d = 0$).

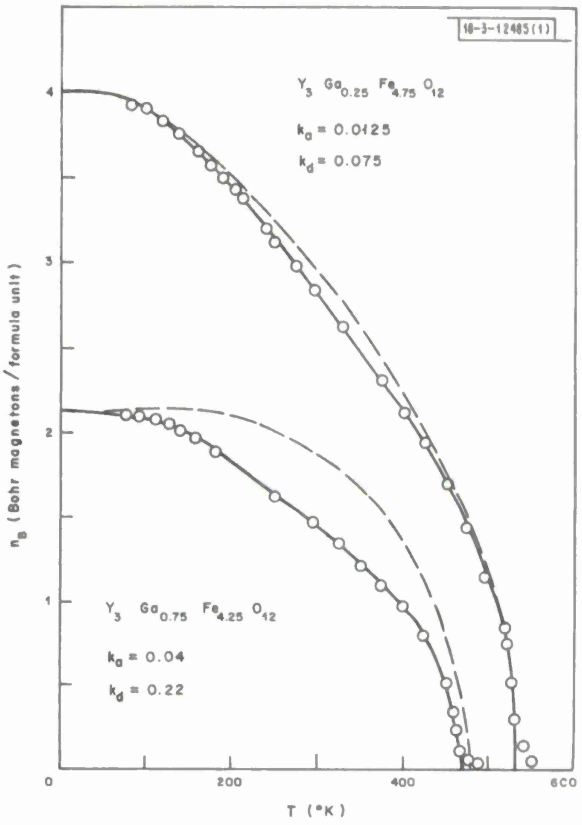

Fig. 8. Comparison of theory and experiment for magnetic moment-temperature curves of $Y_3Ga_{0.25}Fe_{4.75}O_{12}$ and $Y_3Ga_{0.75}Fe_{4.25}O_{12}$. Dashed lines represent the results calculated by using the molecular field coefficients of pure $Y_3Fe_5O_{12}$.

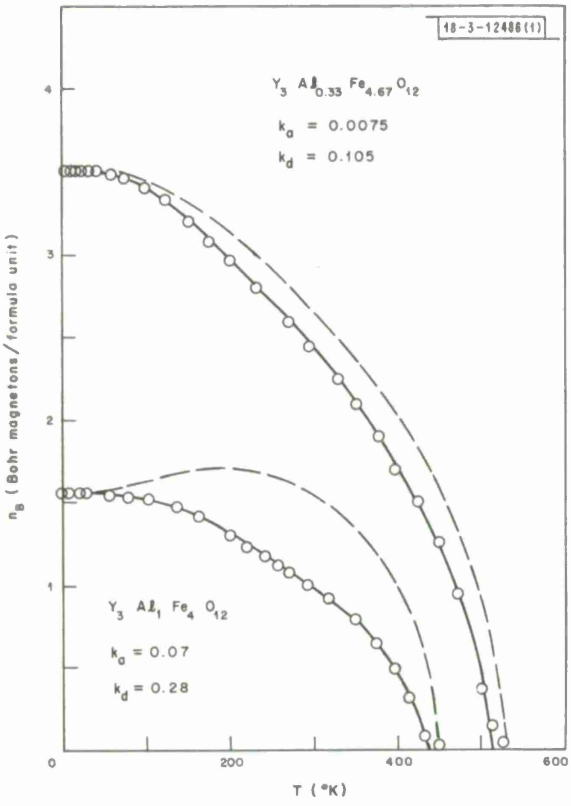

Fig. 9. Comparison of theory and experiment for magnetic moment-temperature curves of $Y_3Al_{0.33}Fe_{4.67}O_{12}$ and $Y_3Al_1Fe_4O_{12}$. Dashed lines represent the results calculated by using the molecular field coefficients of pure $Y_3Fe_5O_{12}$.

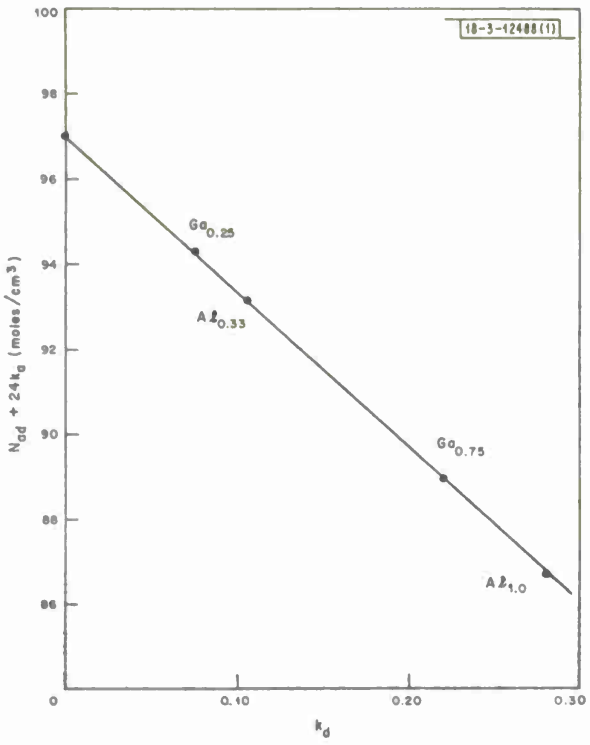

Fig. 10. Linear variation of $N_{ad} + 24k_a$ with k_d.

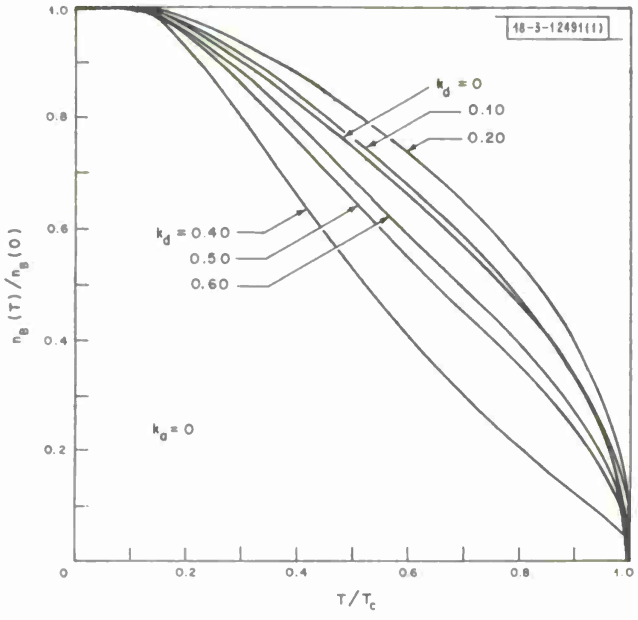

Fig. 11. Theoretical normalized variations of magnetic moment with temperature for pure tetrahedral site substitutions.

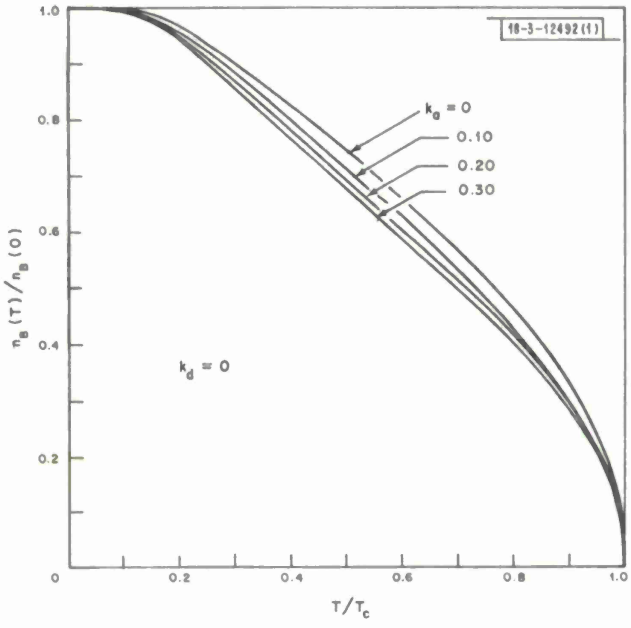

Fig. 12. Theoretical normalized variations of magnetic moment with temperature for pure octahedral site substitutions.

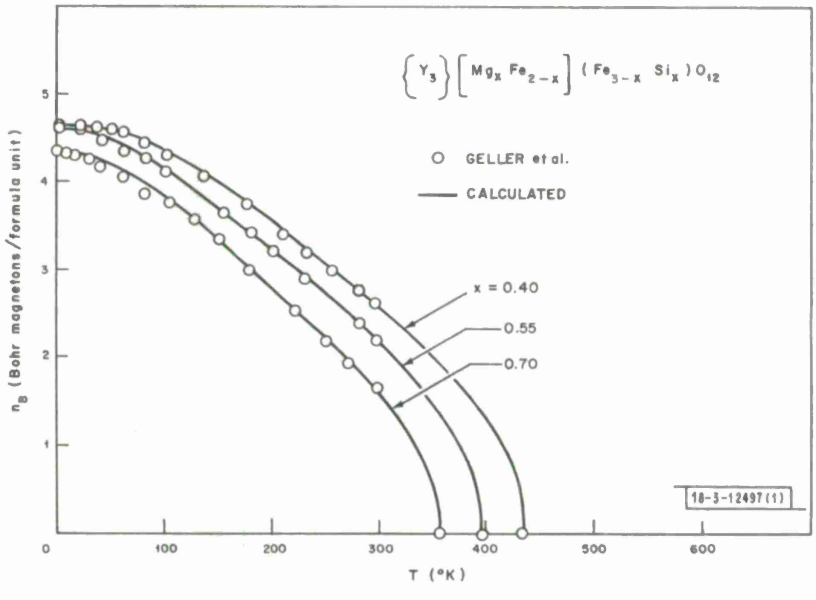

Fig. 13. Comparison of theory with experiment for three compositions of $\{Y_3\}[Mg_xFe_{2-x}](Fe_{3-x}Si_x)O_{12}$, which feature substitutions in both sublattices.

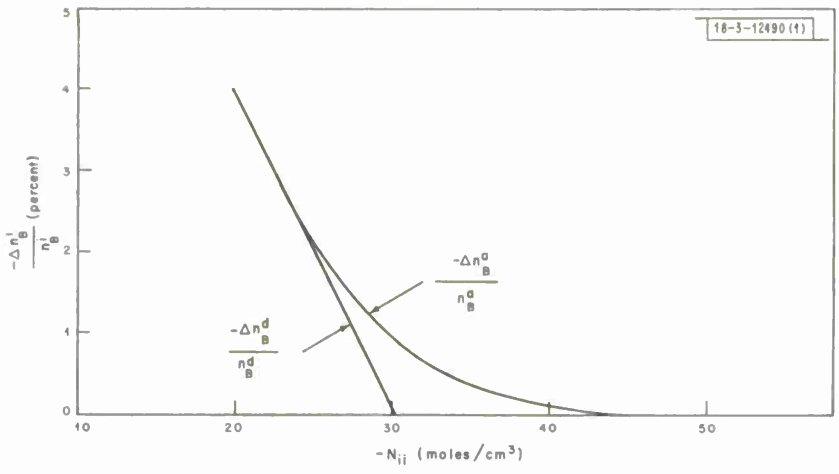

Fig. 14. Percent change in sublattice magnetic moment (attributed to canting) as a function of the sublattice molecular field coefficient. At $N_{ii} \simeq -20$ moles/cm^3, antiferromagnetic transitions occur in both cases.

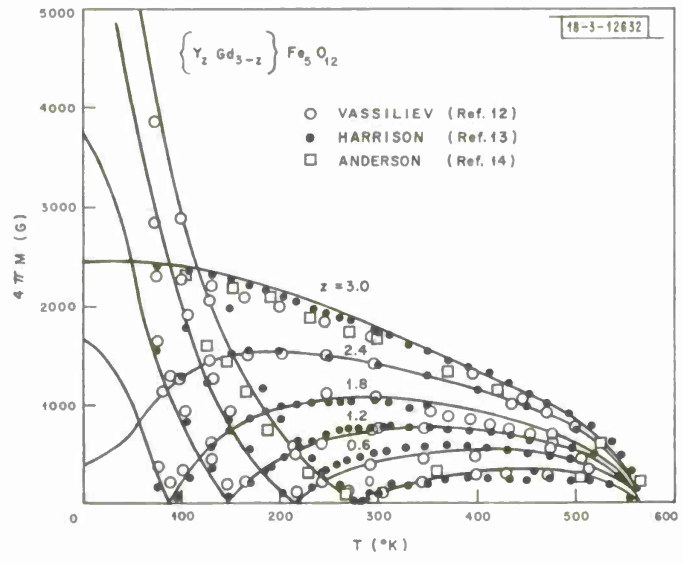

Fig. 15. Comparison of theory and experiment for magnetization-temperature curves of $Y_zGd_{3-z}Fe_5O_{12}$ for z = 0, 0.6, 1.2, 1.8, 2.4, and 3.0.

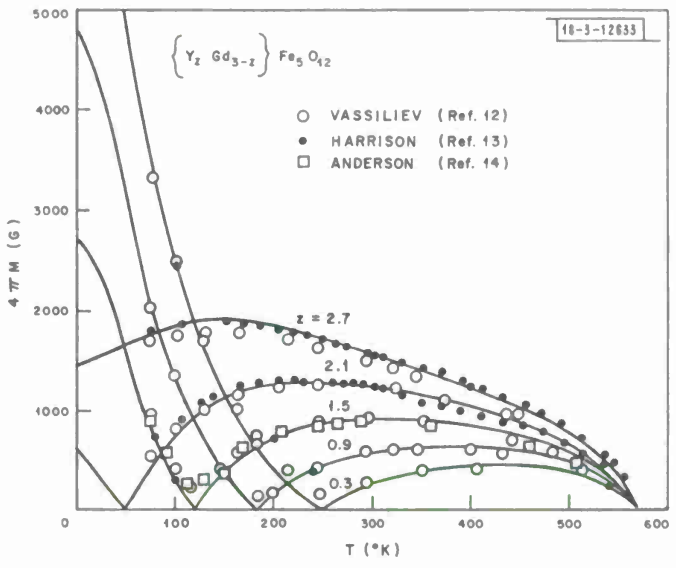

Fig. 16. Comparison of theory and experiment for magnetization-temperature curves of $Y_zGd_{3-z}Fe_5O_{12}$ for z = 0.3, 0.9, 1.5, 2.1, and 2.7.

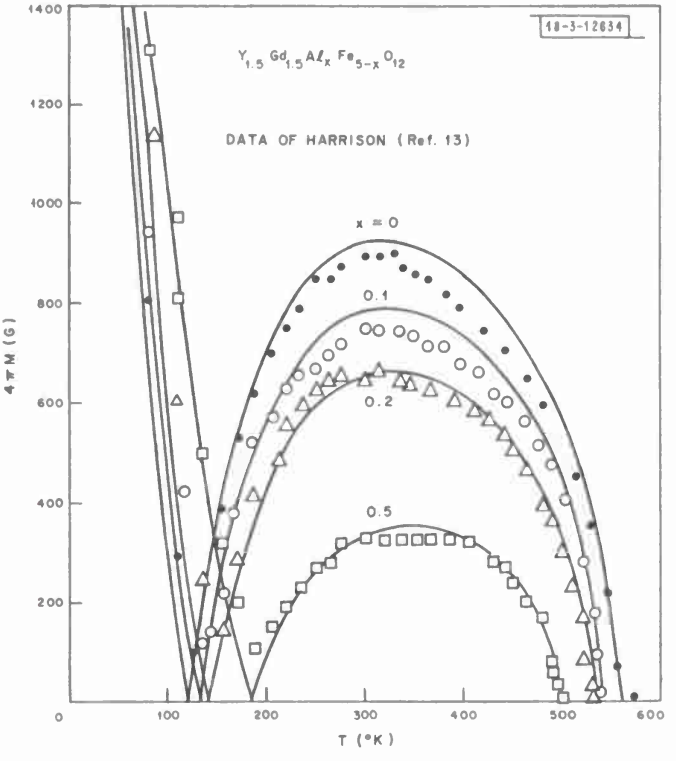

Fig. 17. Comparison of theory and experiment for magnetization-temperature curves of $Y_{1.5}Gd_{1.5}Al_xFe_{5-x}O_{12}$ for x = 0, 0.1, 0.2, and 0.5.

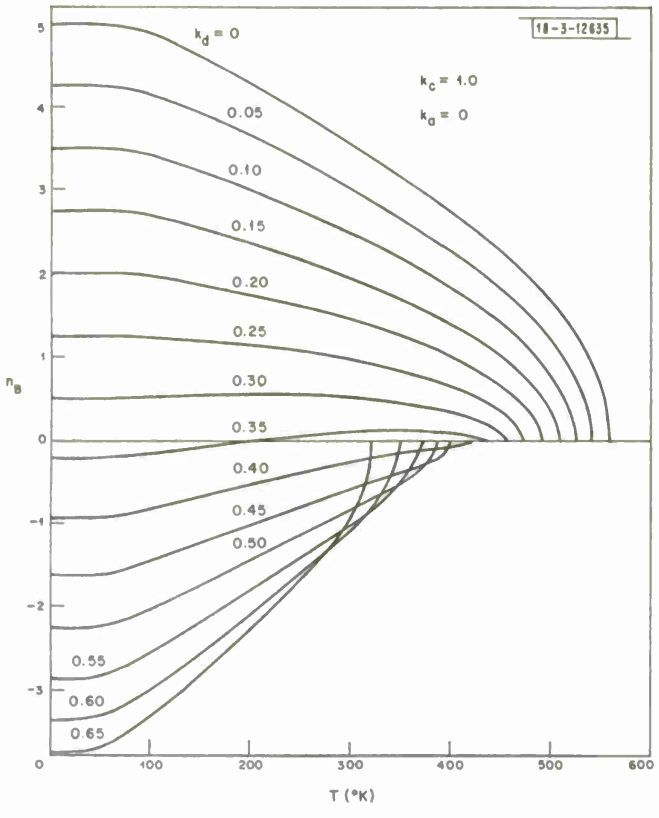

(a) For $k_a = 0$.

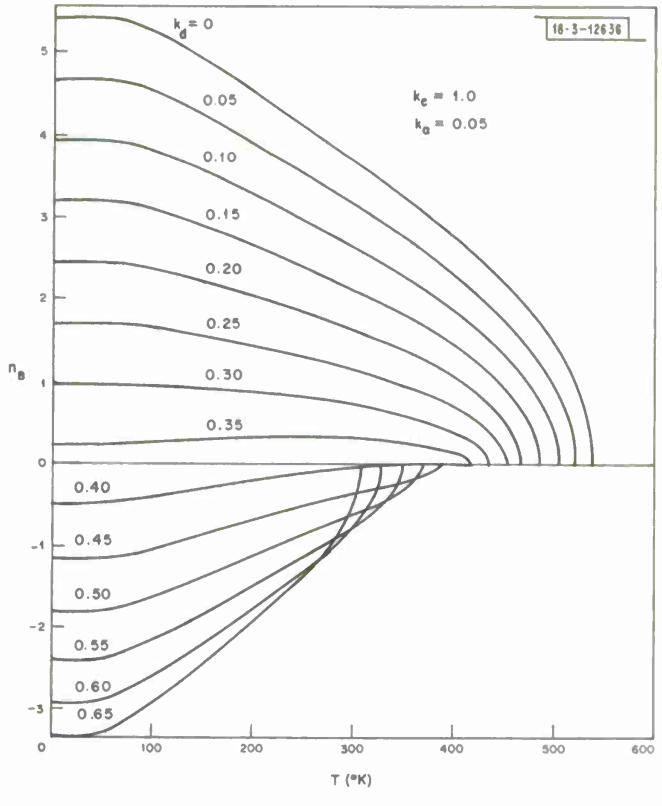

(b) For $k_a = 0.05$.

Fig. 18(a-h). Magnetic moment n_B vs T for $k_c = 1.0$, $0 \leqslant k_d \leqslant 0.65$, k_a (as indicated).

(c) For $k_a = 0.10$.

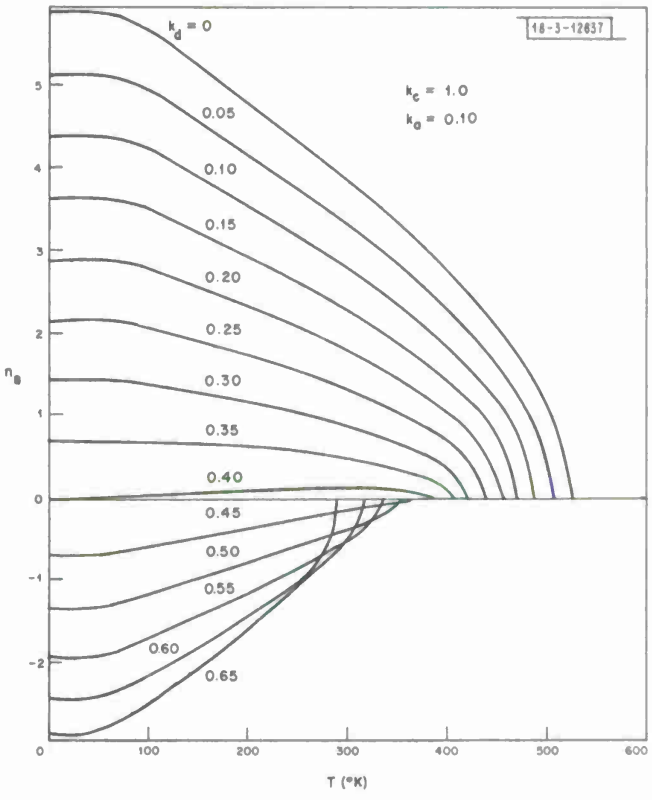

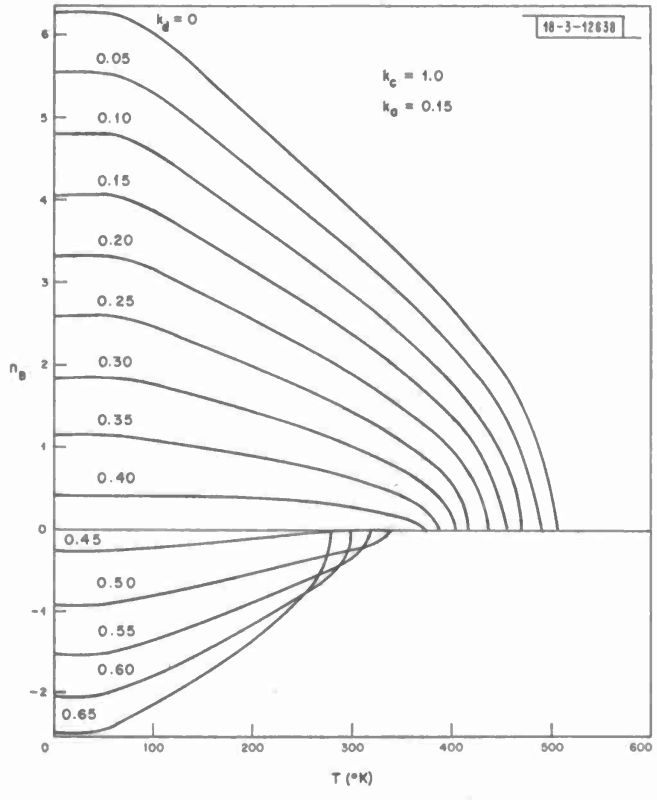

(d) For $k_a = 0.15$.

Fig. 18(a-h). Continued.

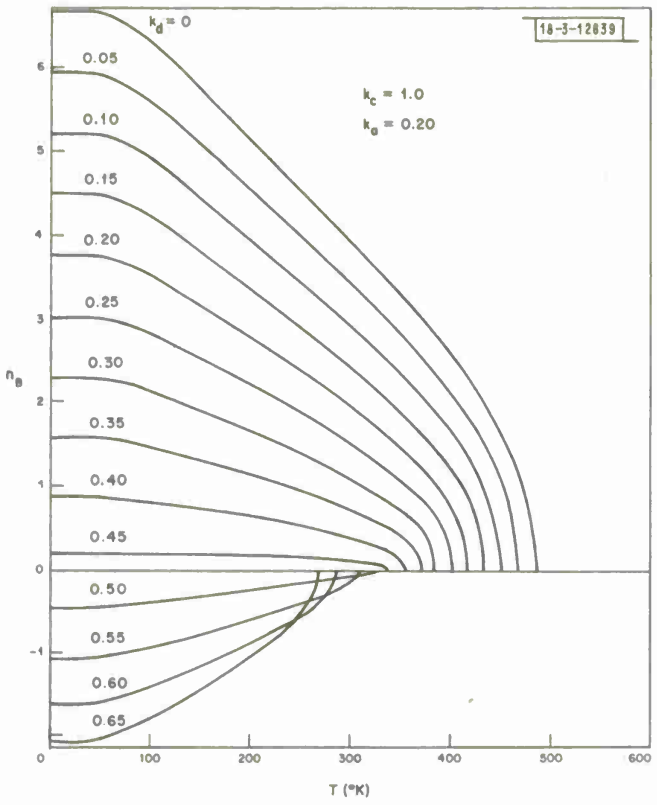

(e) For $k_a = 0.20$.

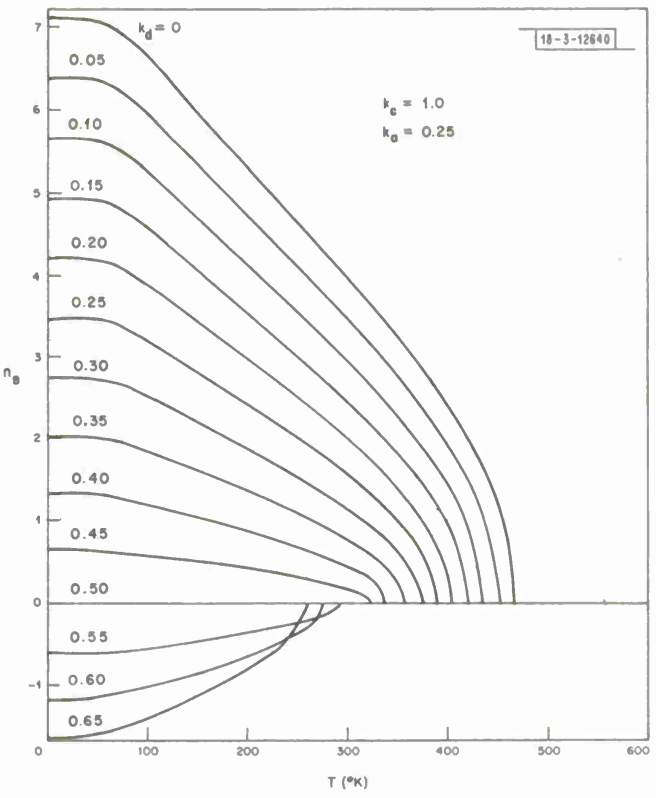

(f) For $k_a = 0.25$.

Fig. 18(a-h). Continued.

(g) For $k_a = 0.30$.

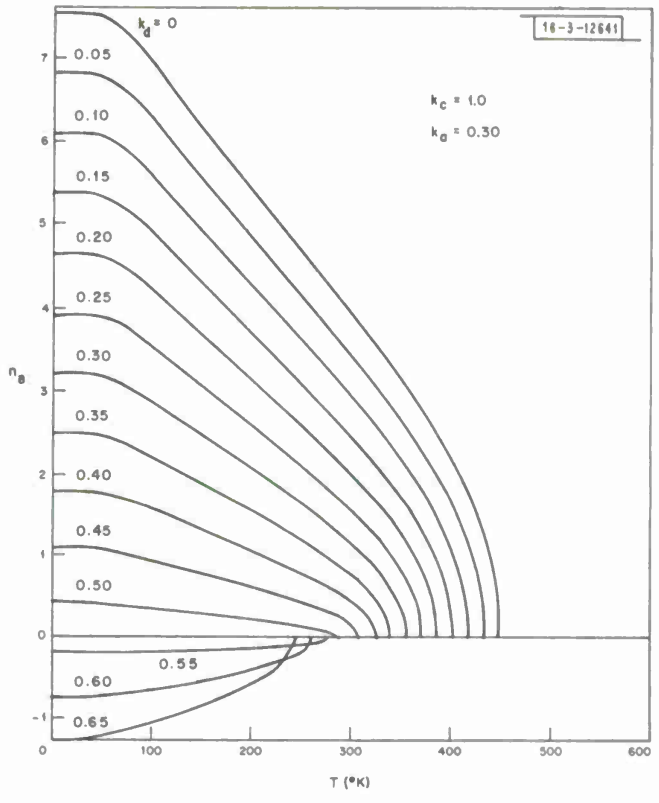

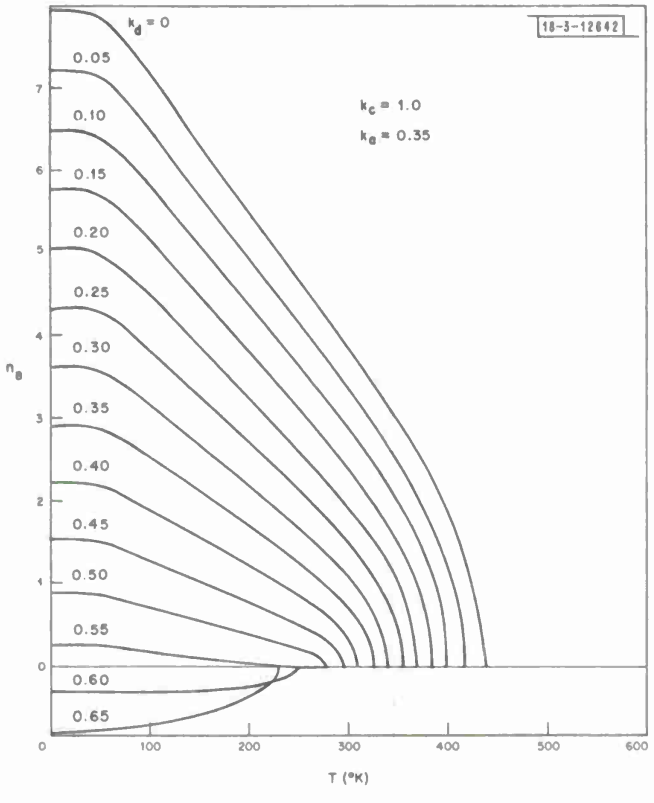

(h) For $k_a = 0.35$.

Fig. 18(a-h). Continued.

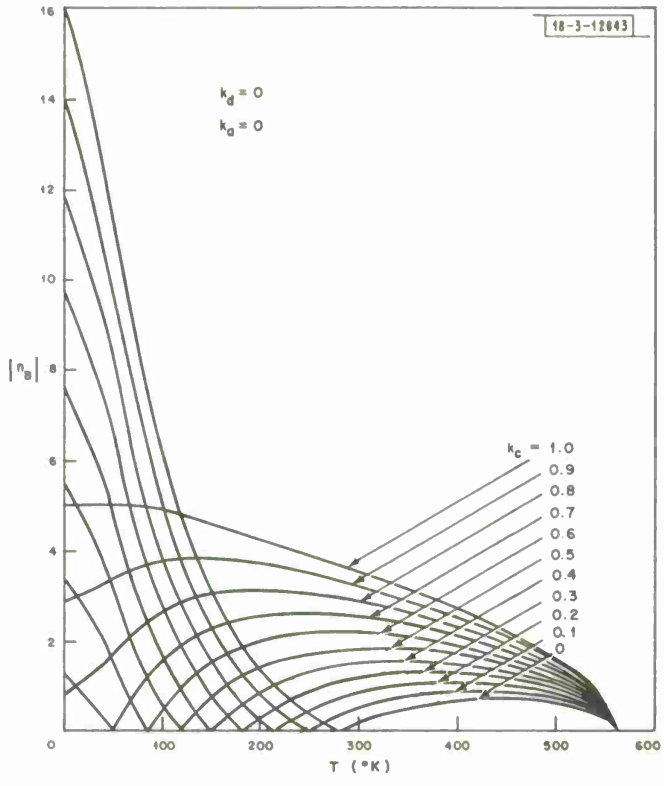

Fig. 19. Magnetic moment $|n_B|$ vs T for $k_d = k_a = 0$, $0 \leqslant k_c \leqslant 1.0$.

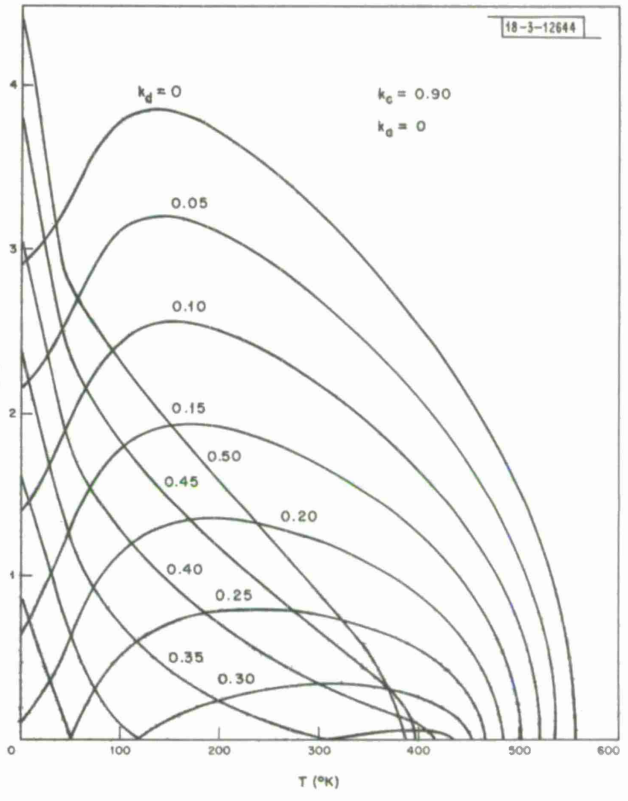

(a) For $k_a = 0$.

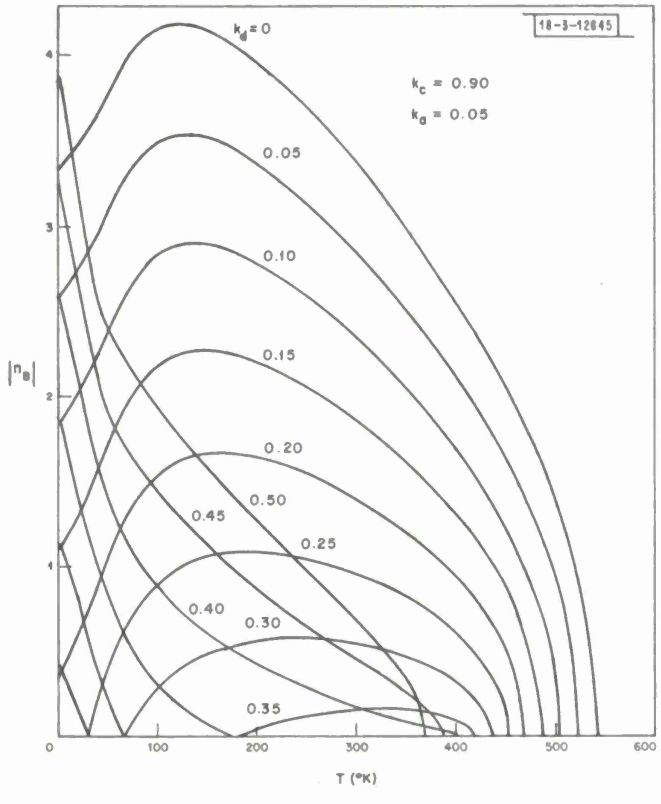

(b) For $k_a = 0.05$.

Fig. 20(a-h). Magnetic moment $|n_B|$ vs T for $k_c = 0.90$, $0 \leqslant k_d \leqslant 0.50$, k_a (as indicated).

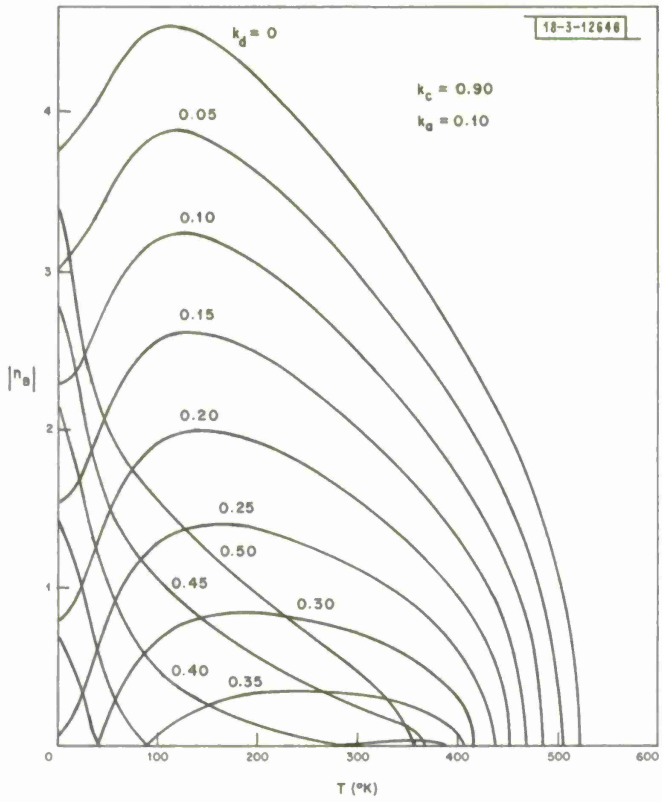

(c) For $k_a = 0.10$.

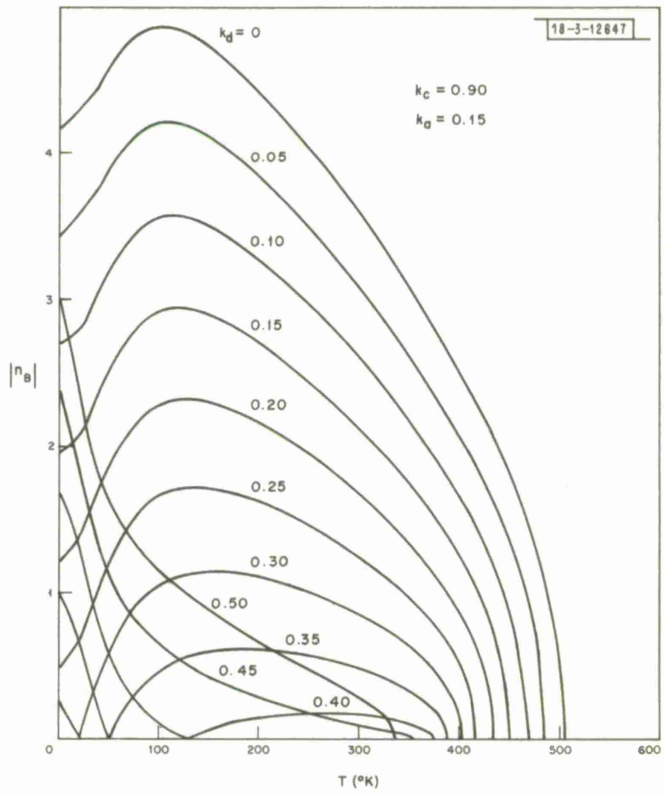

(d) For $k_a = 0.15$.

Fig. 20(a-h). Continued.

(e) For $k_a = 0.20$.

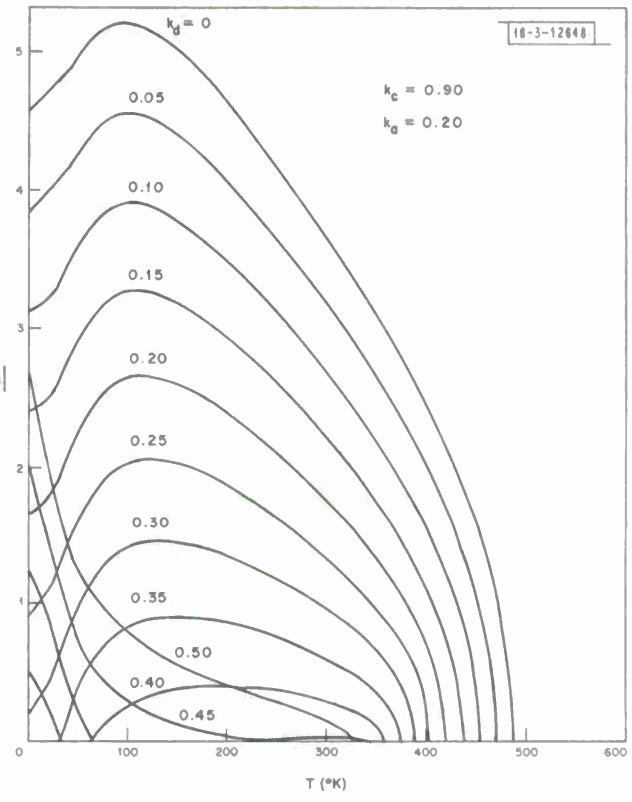

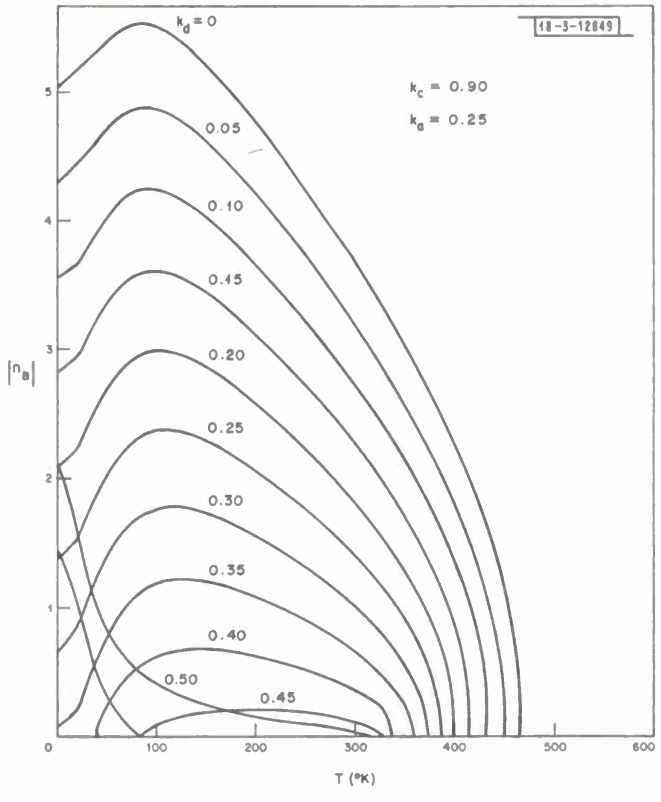

(f) For $k_a = 0.25$.

Fig. 20(a-h). Continued.

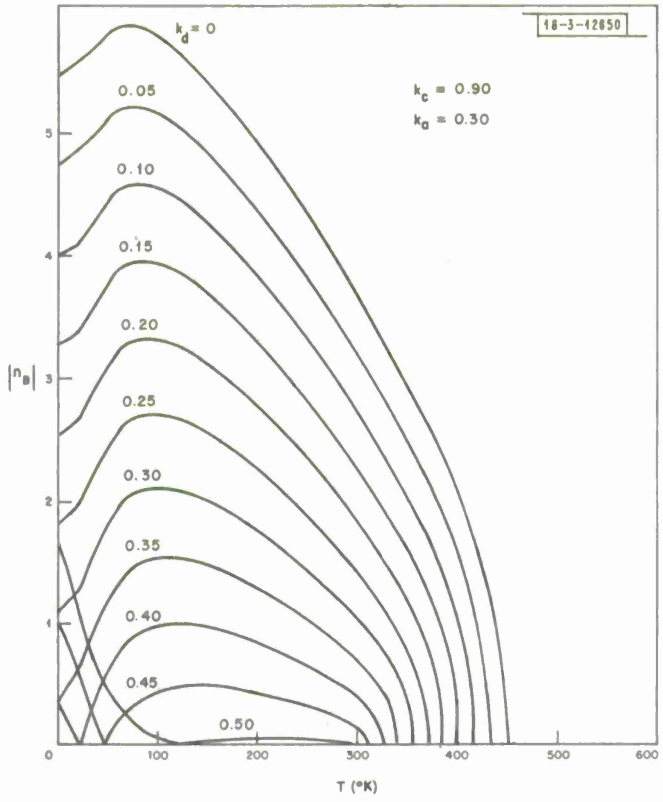

(g) For $k_a = 0.30$.

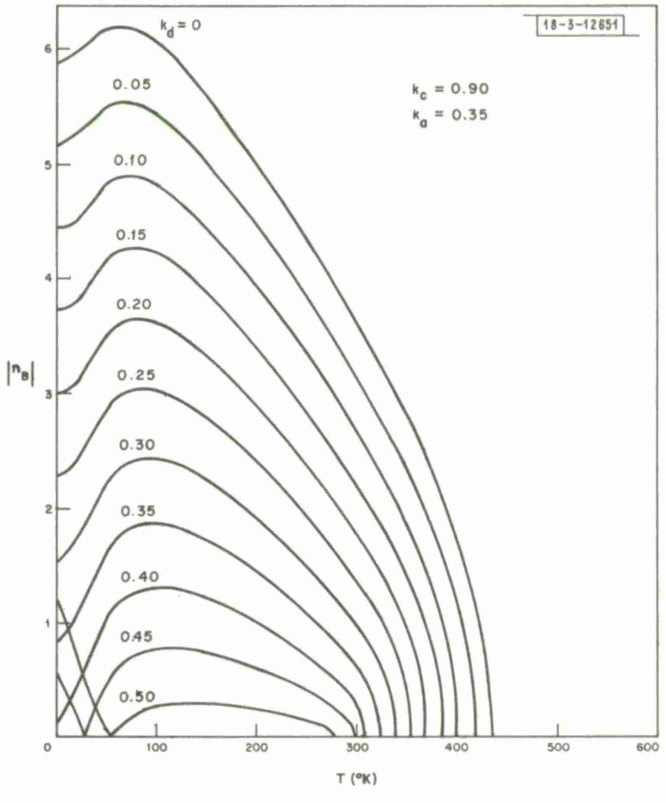

(h) For $k_a = 0.35$.

Fig. 20(a-h). Continued.

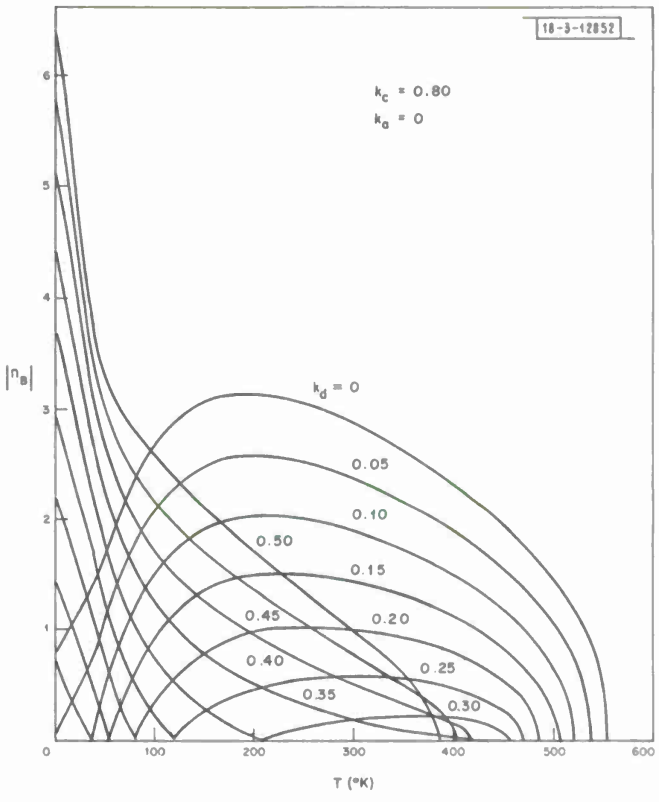

(a) For $k_a = 0$.

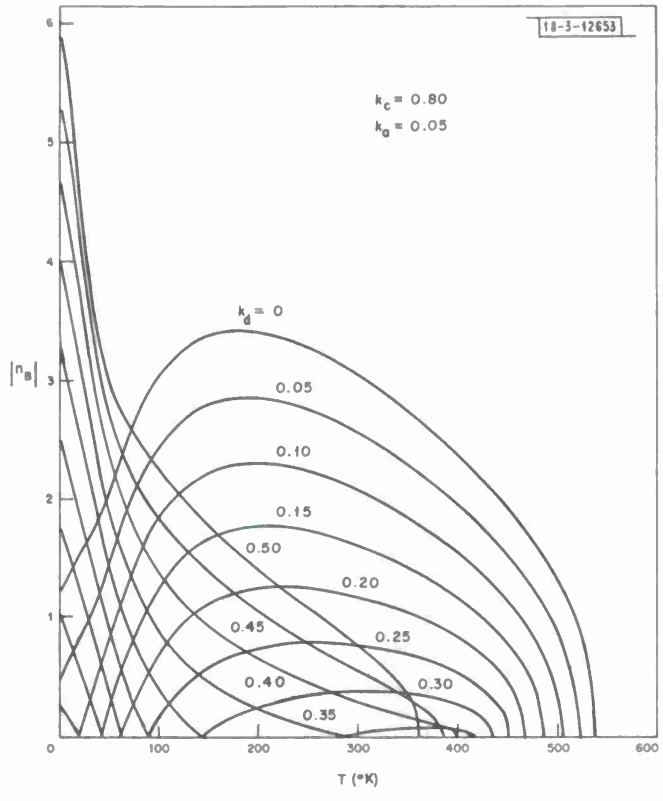

(b) For $k_a = 0.05$.

Fig. 21(a-h). Magnetic moment $|n_B|$ vs T for $k_c = 0.80$, $0 \leqslant k_d \leqslant 0.50$, k_a (as indicated).

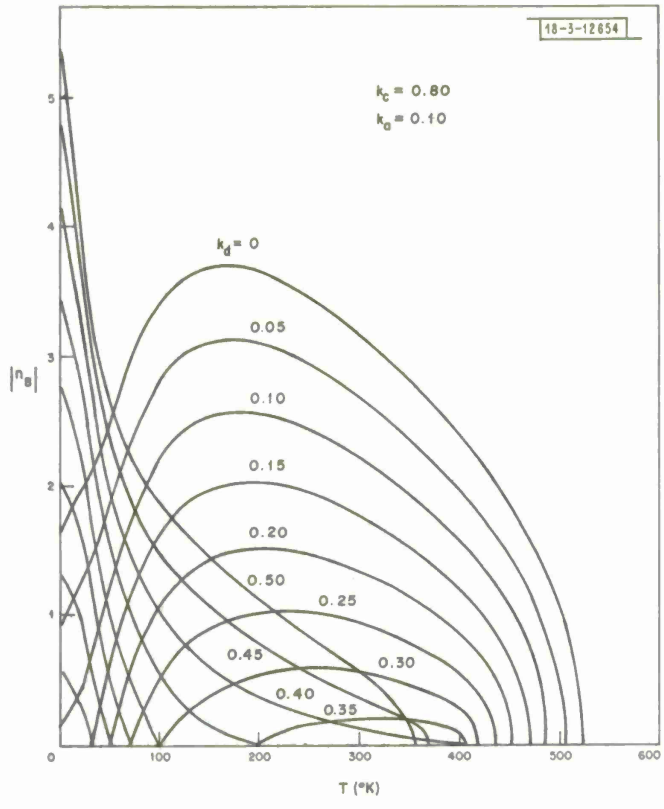

(c) For $k_a = 0.10$.

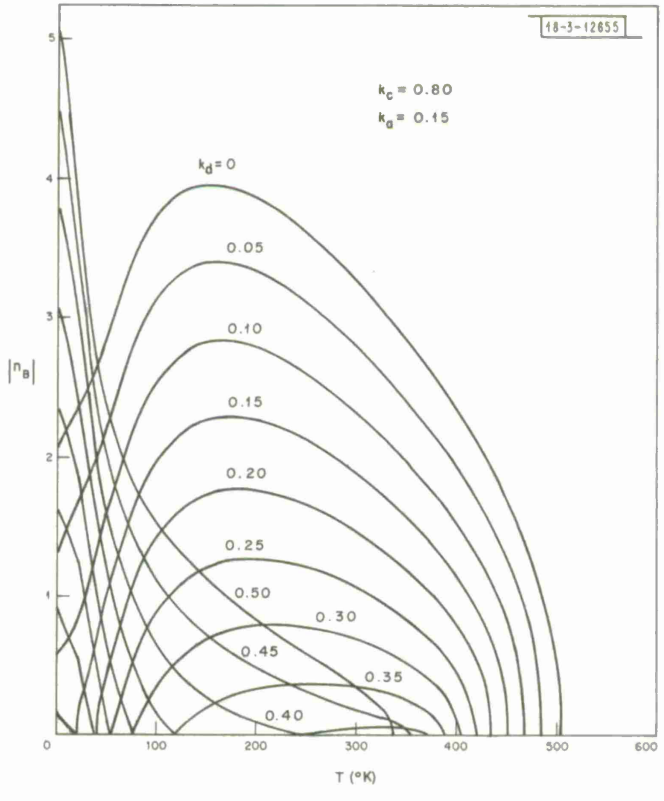

(d) For $k_a = 0.15$.

Fig. 21(a-h). Continued.

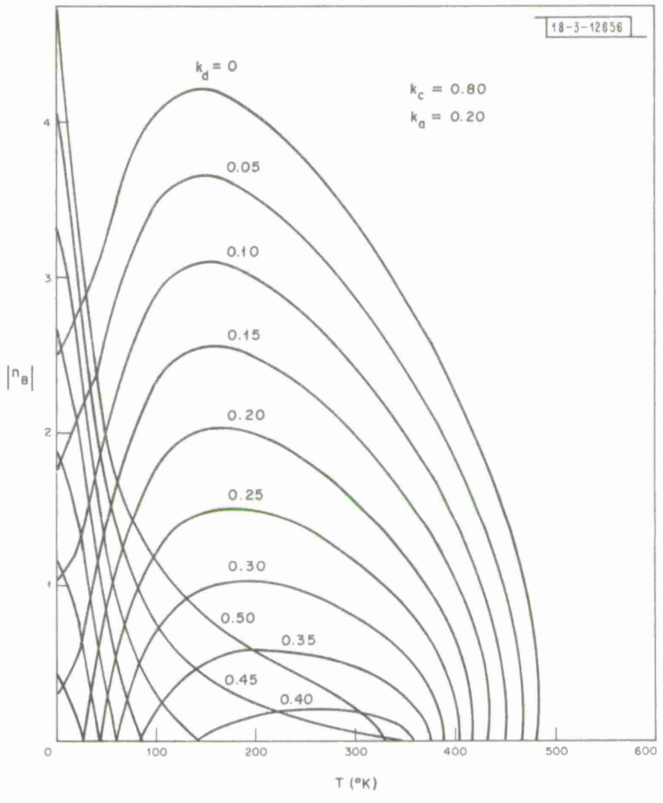

(e) For $k_a = 0.20$.

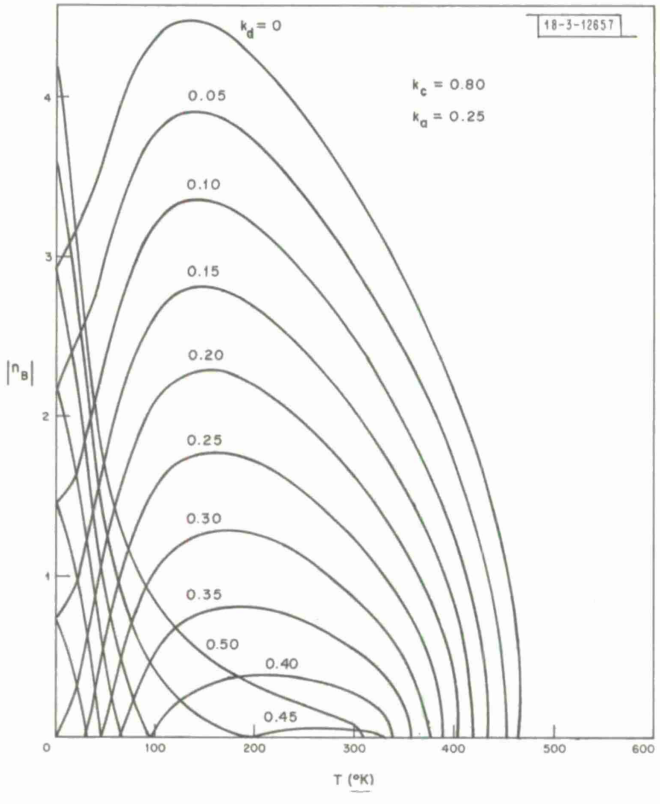

(f) For $k_a = 0.25$.

Fig. 21(a-h). Continued.

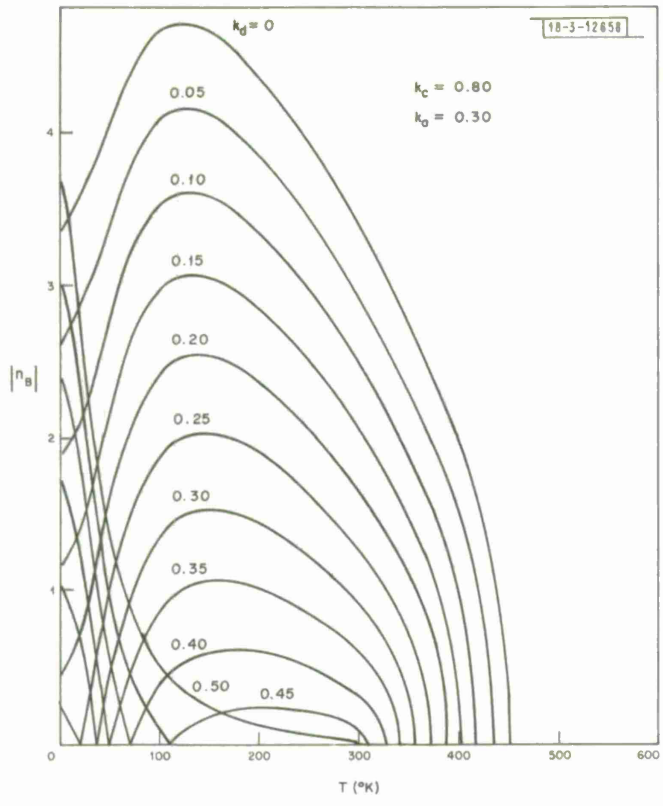

(g) For $k_a = 0.30$.

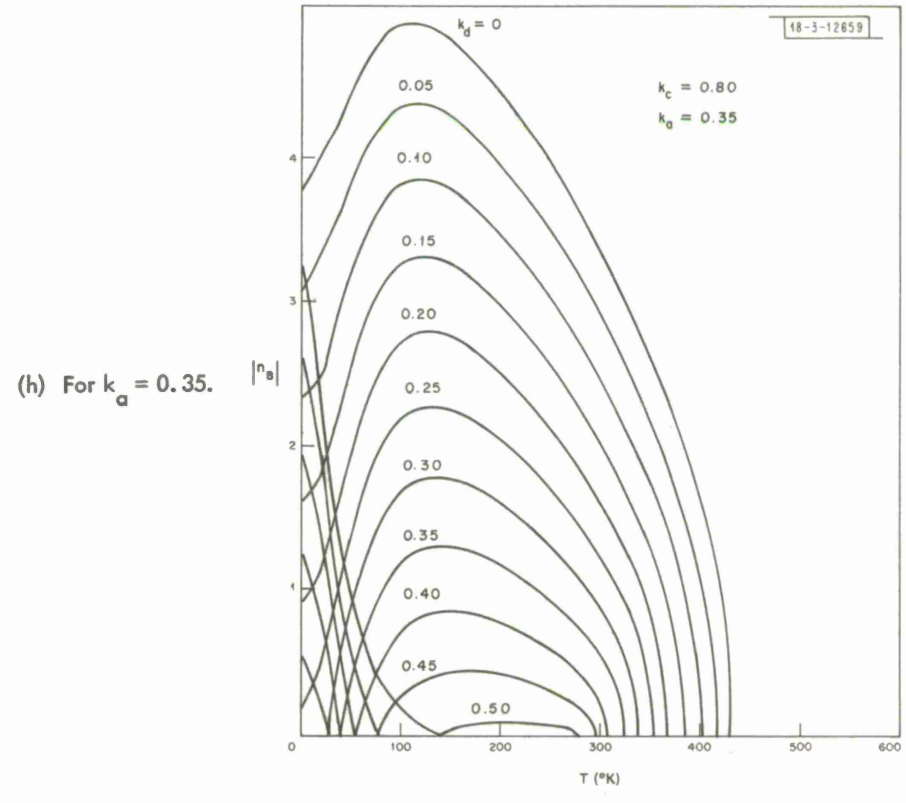

(h) For $k_a = 0.35$.

Fig. 21(a-h). Continued.

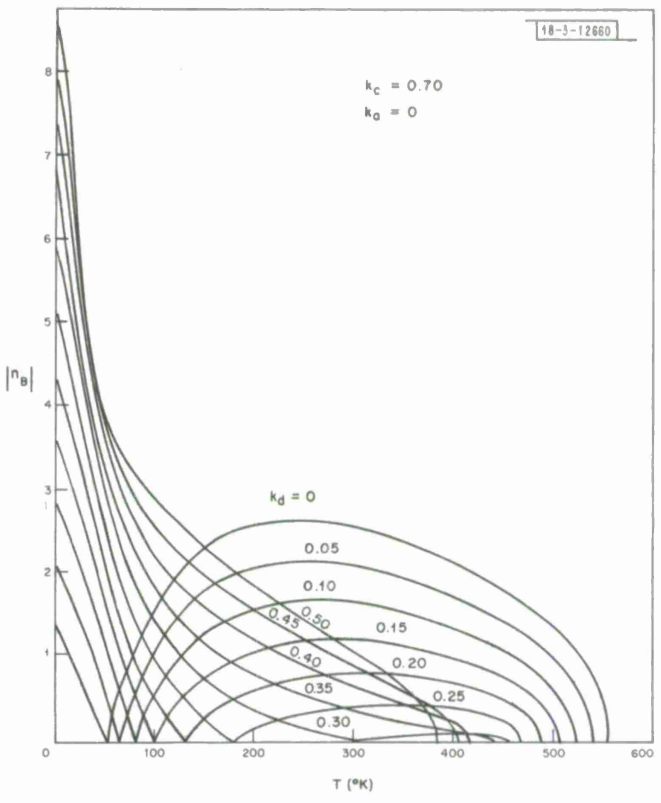

(a) For $k_a = 0$.

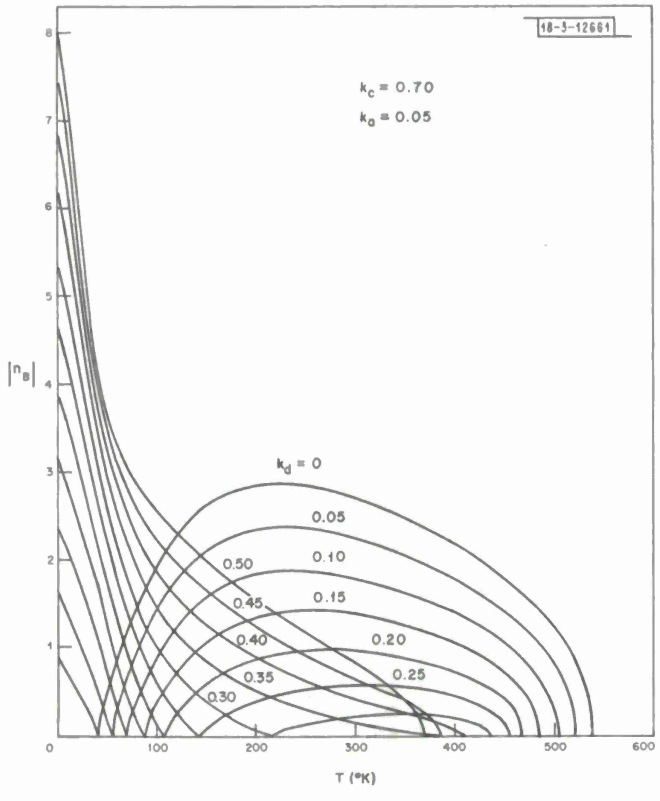

(b) For $k_a = 0.05$.

Fig. 22(a-h). Magnetic moment $|n_B|$ vs T for $k_c = 0.70$, $0 \leqslant k_d \leqslant 0.50$, k_a (as indicated).

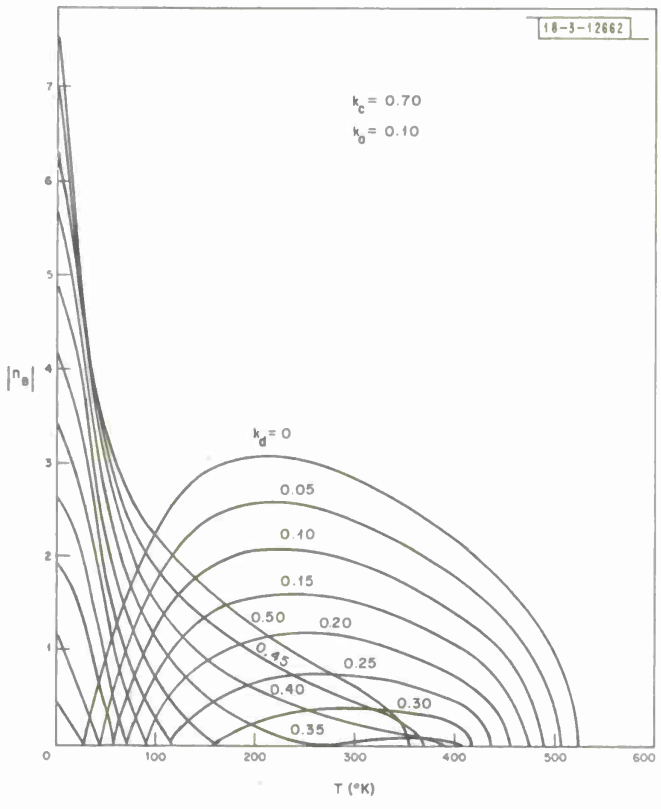

(c) For $k_a = 0.10$.

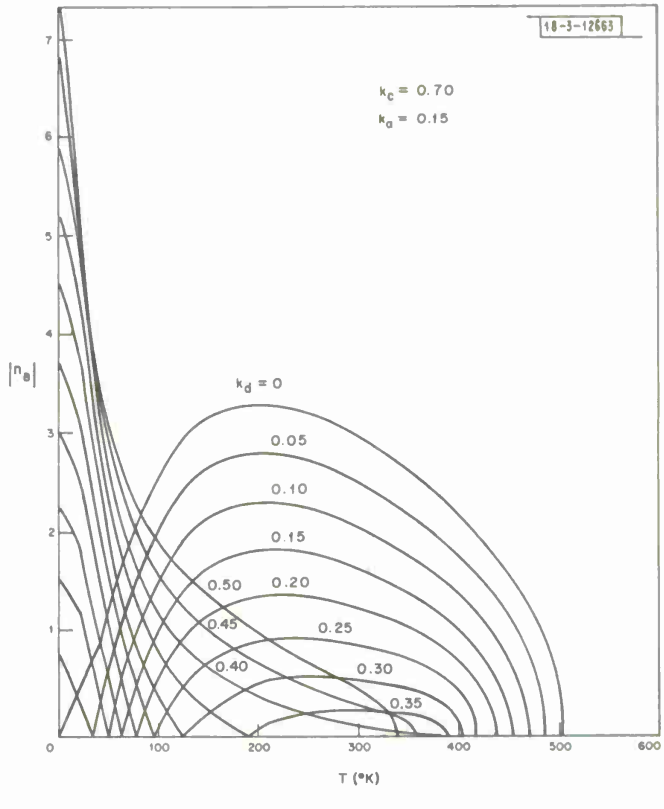

(d) For $k_a = 0.15$.

Fig. 22(a-h). Continued.

(e) For $k_a = 0.20$.

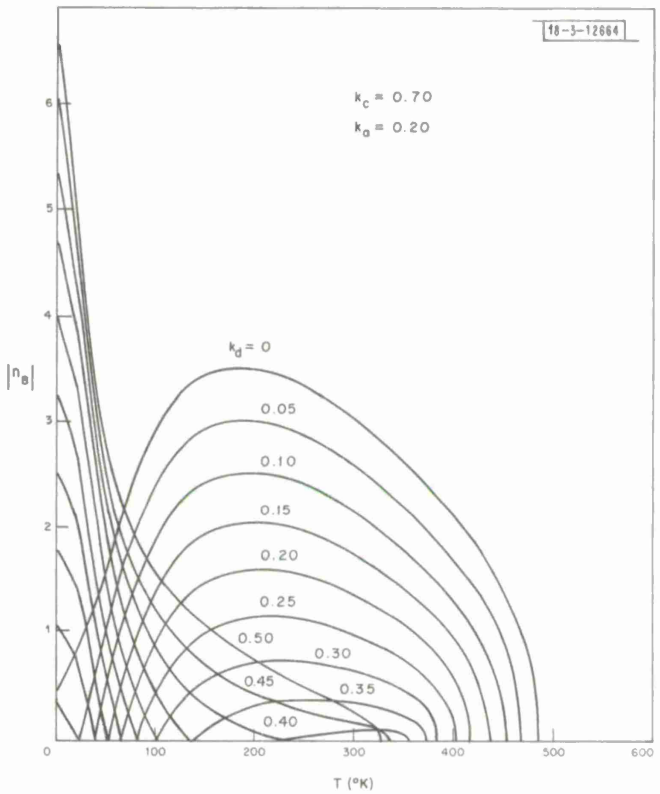

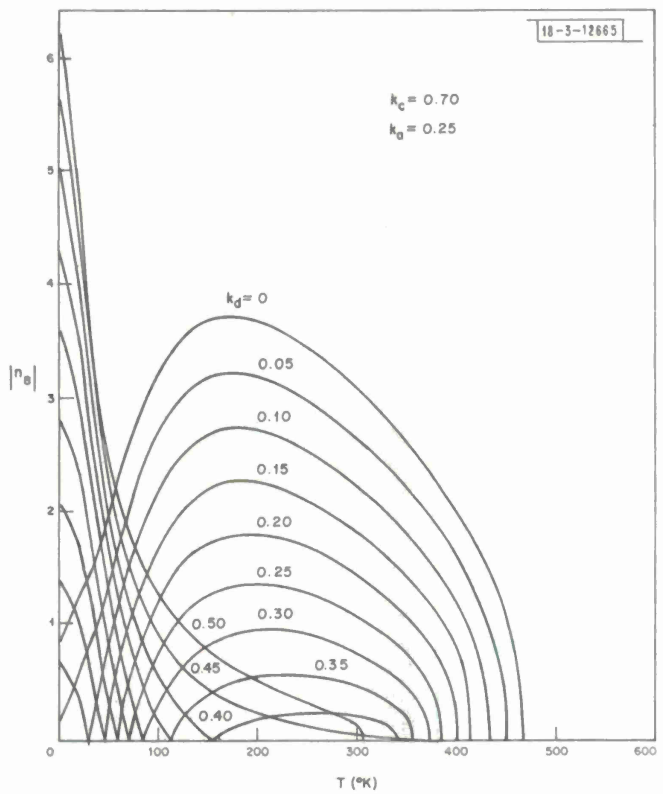

(f) For $k_a = 0.25$.

Fig. 22(a-h). Continued.

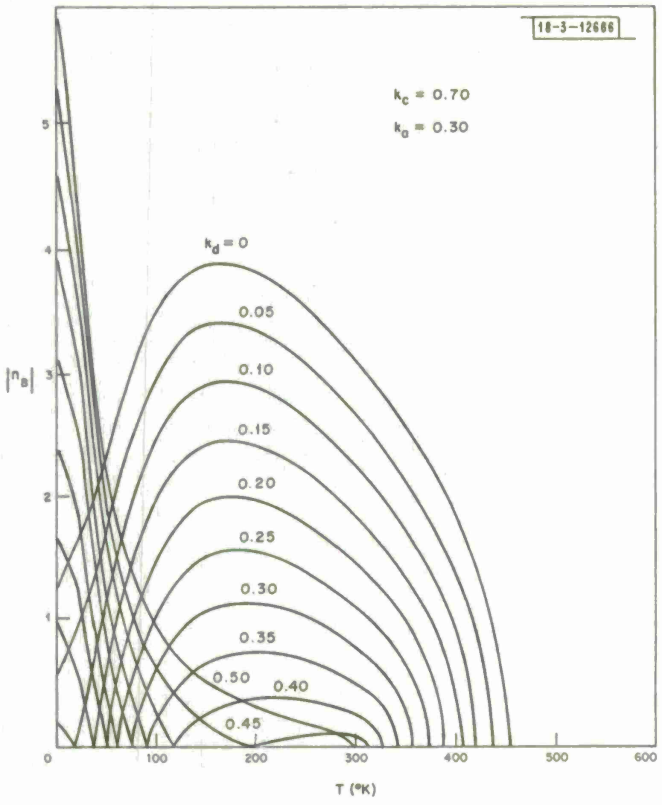

(g) For $k_a = 0.30$.

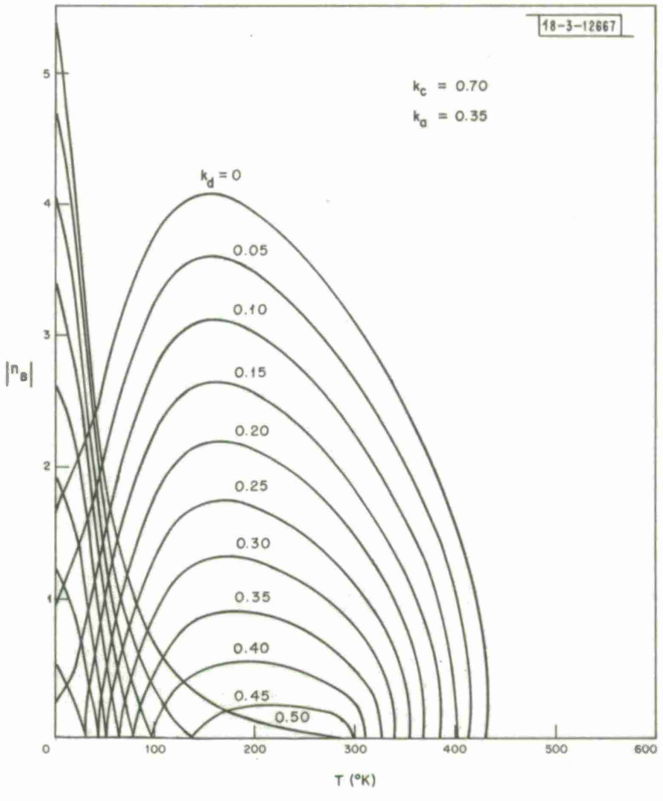

(h) For $k_a = 0.35$.

Fig. 22(a-h). Continued.

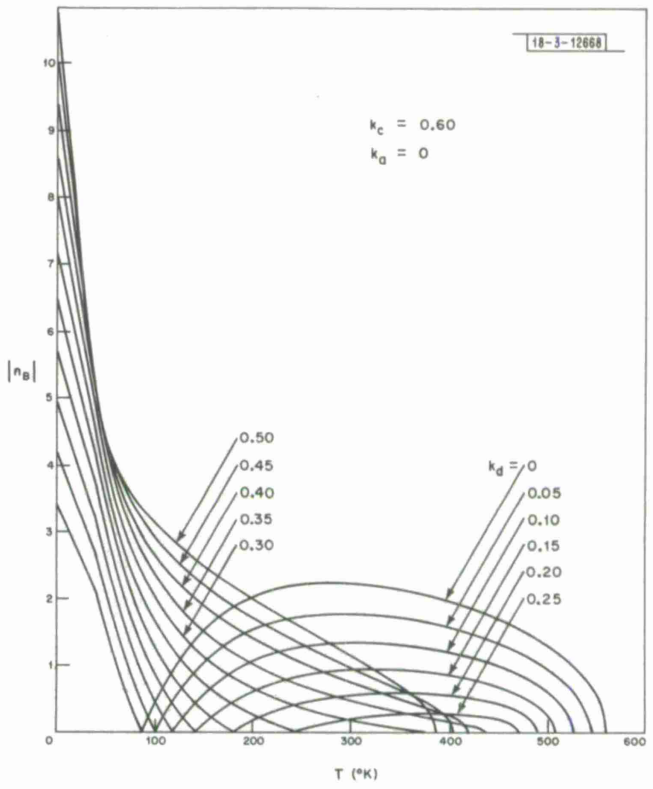

(a) For $k_a = 0$.

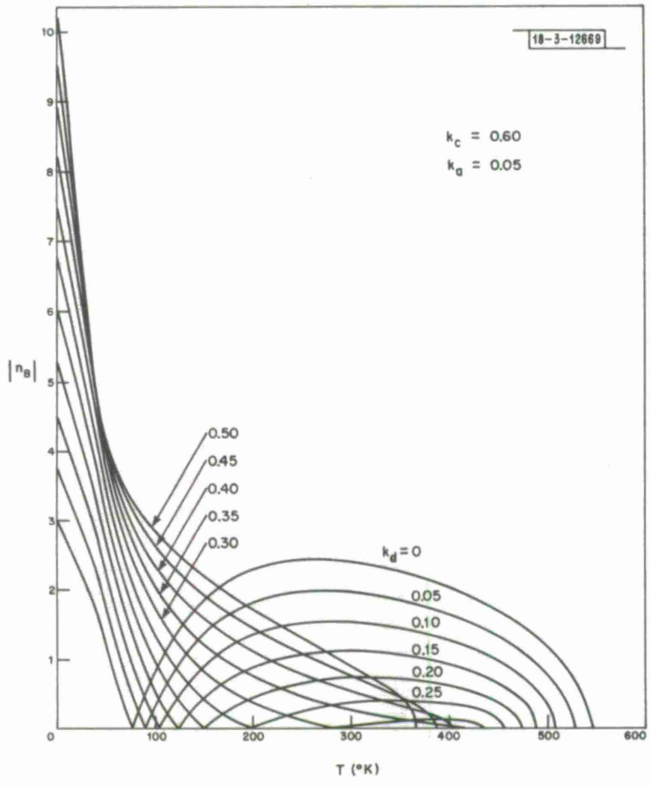

(b) For $k_a = 0.05$.

Fig. 23(a-h). Magnetic moment $|n_B|$ vs T for $k_c = 0.60$, $0 \leqslant k_d \leqslant 0.50$, k_a (as indicated).

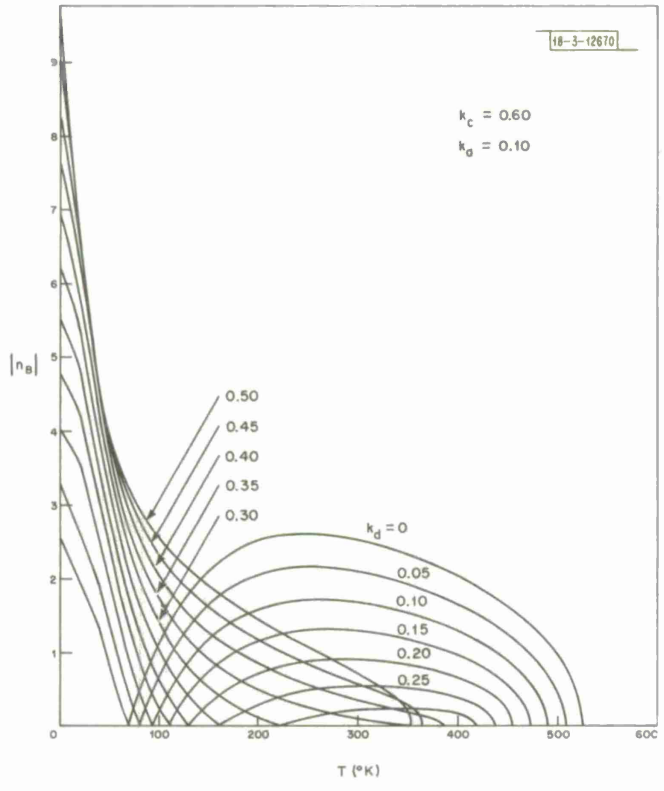

(c) For $k_a = 0.10$.

(d) For $k_a = 0.15$.

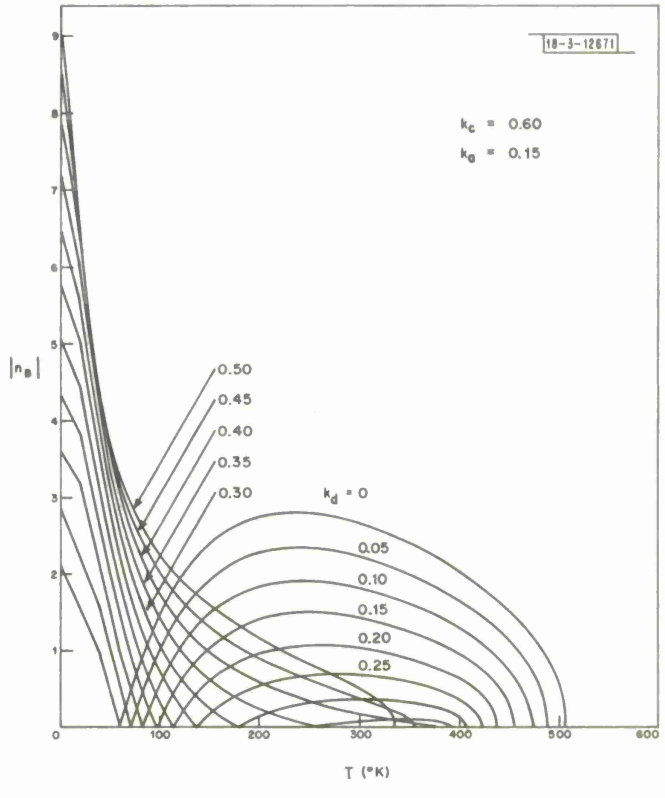

Fig. 23(a-h). Continued.

(e) For $k_a = 0.20$.

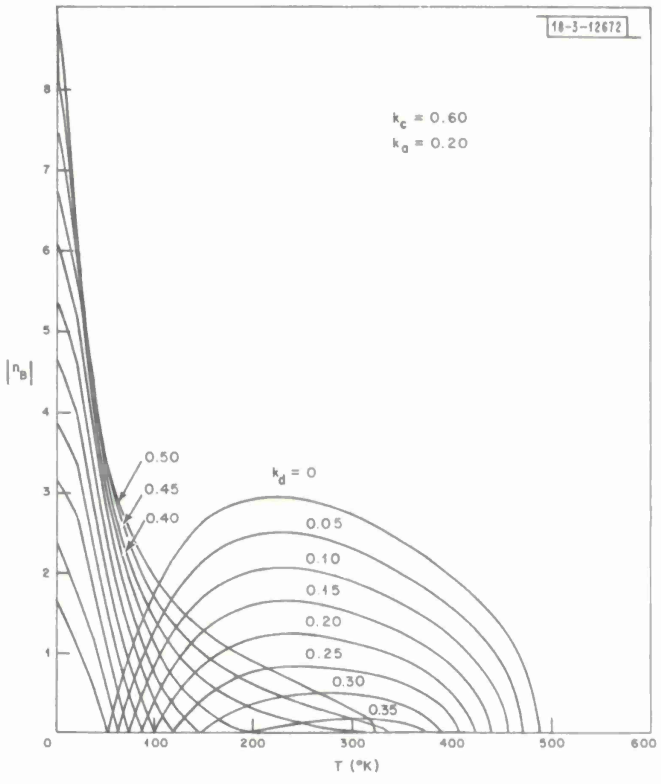

(f) For $k_a = 0.25$.

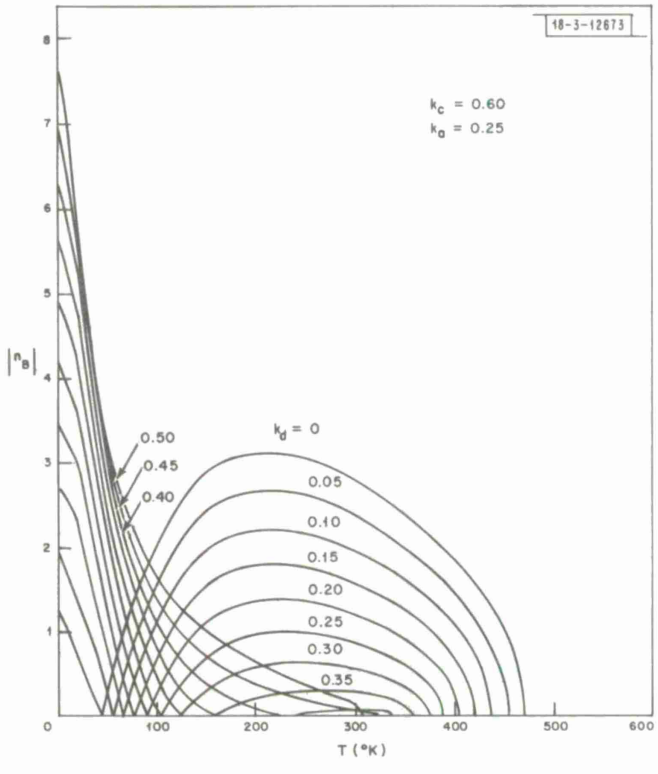

Fig. 23(a-h). Continued.

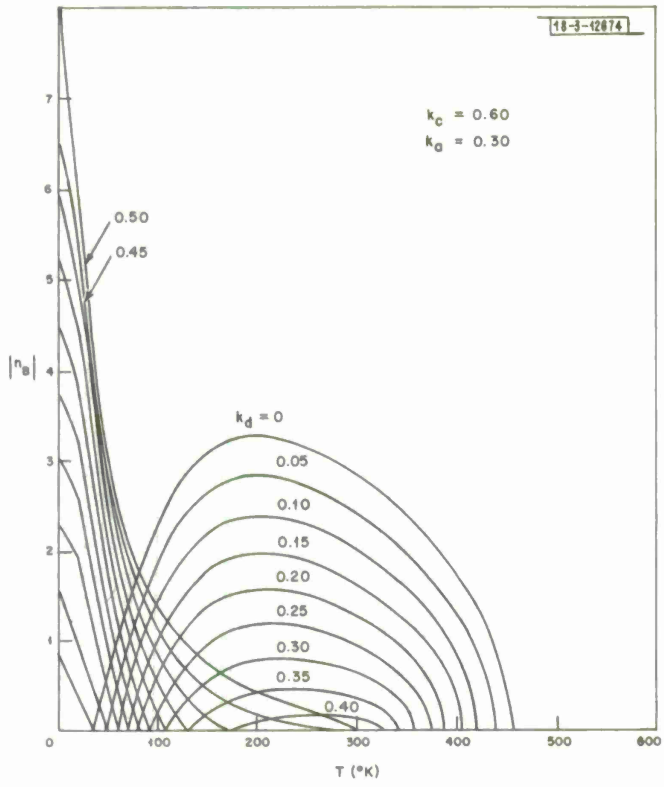

(g) For $k_a = 0.30$.

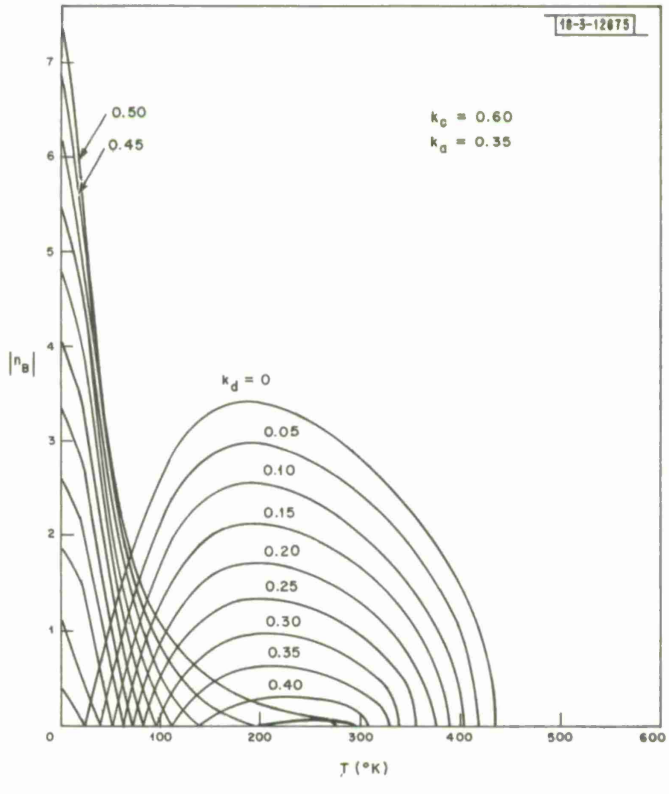

(h) For $k_a = 0.35$.

Fig. 23(a-h). Continued.

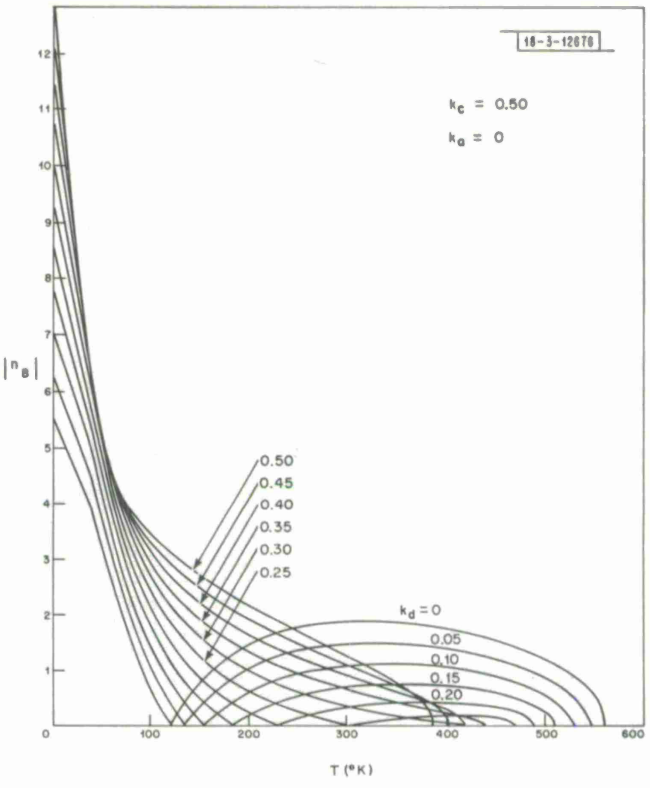

(a) For $k_a = 0$.

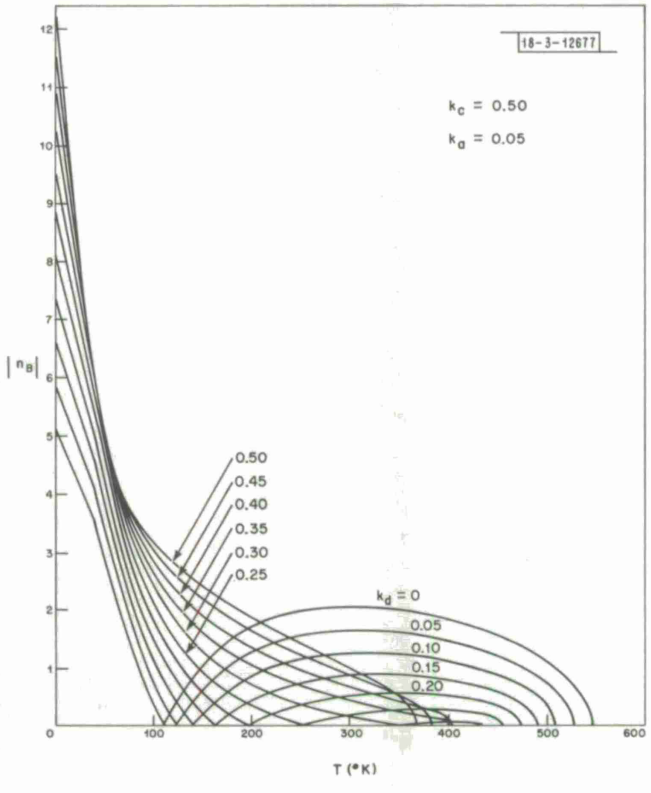

(b) For $k_a = 0.05$.

Fig. 24(a-h). Magnetic moment $|n_B|$ vs T for $k_c = 0.50$, $0 \leqslant k_d \leqslant 0.50$, k_a (as indicated).

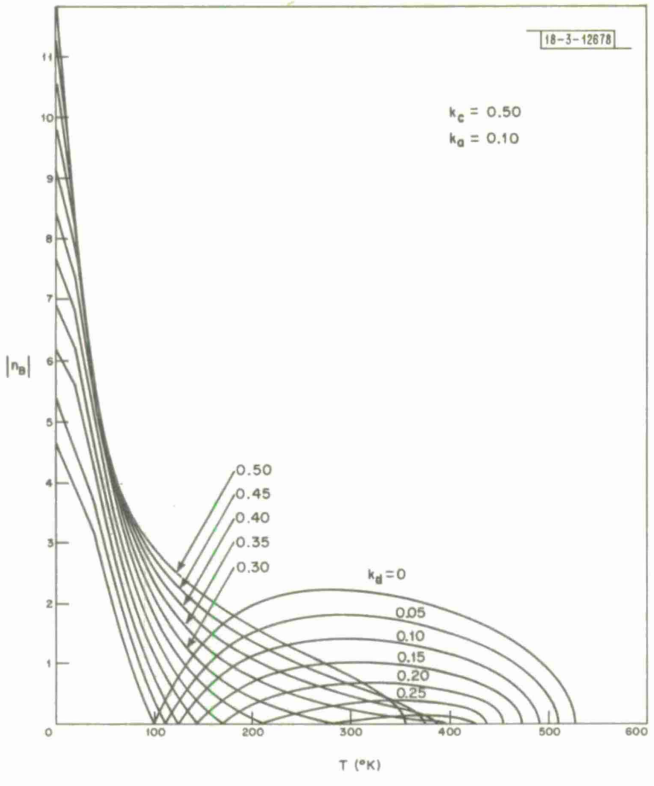

(c) For $k_a = 0.10$.

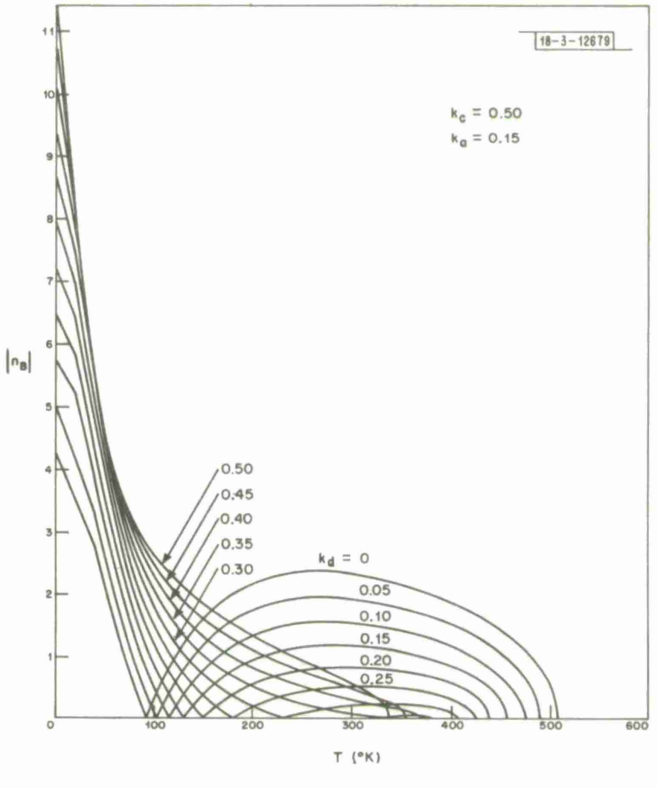

(d) For $k_a = 0.15$.

Fig. 24(a-h). Continued.

(e) For $k_a = 0.20$.

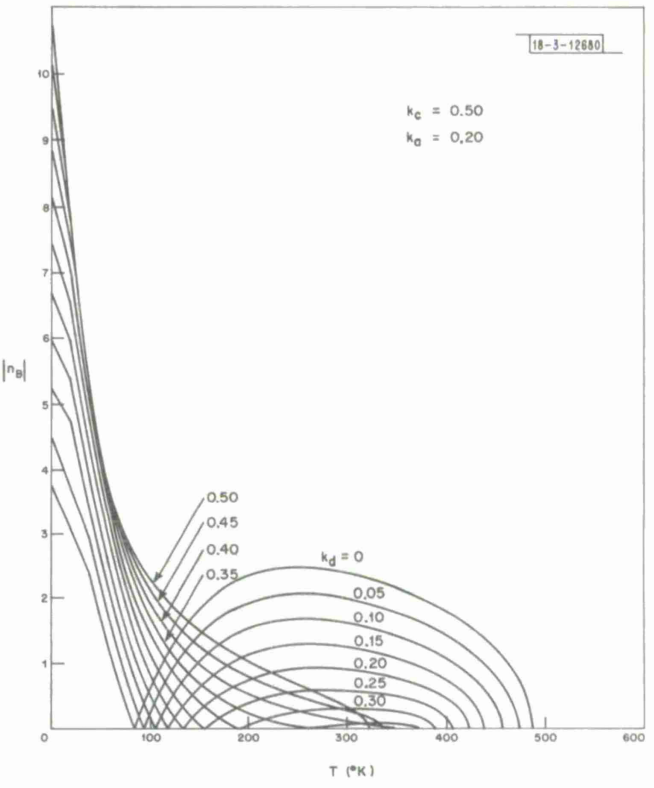

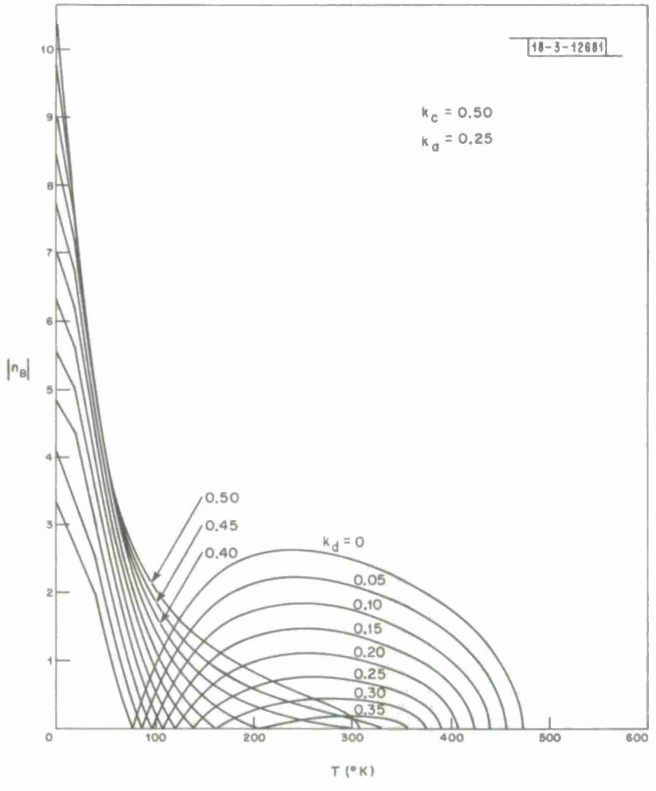

(f) For $k_a = 0.25$.

Fig. 24(a-h). Continued.

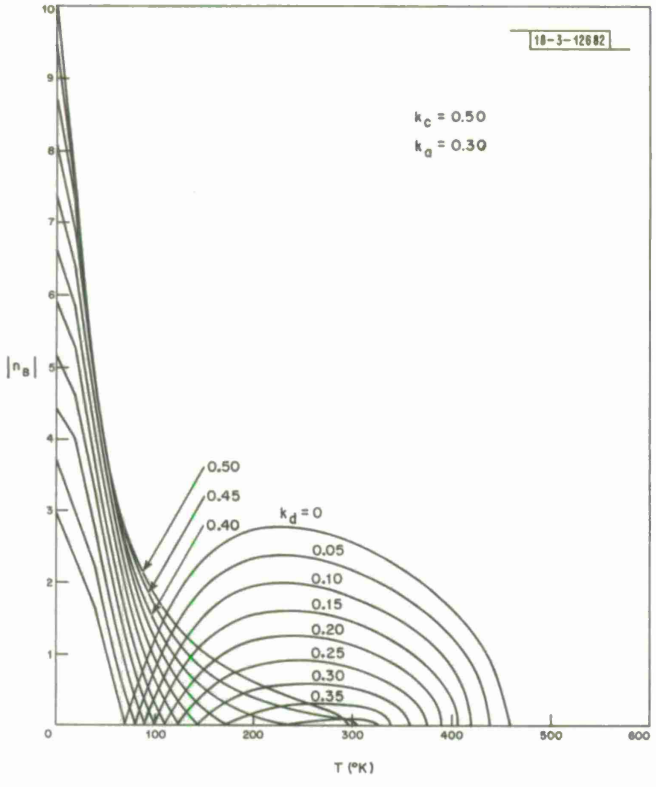

(g) For $k_a = 0.30$.

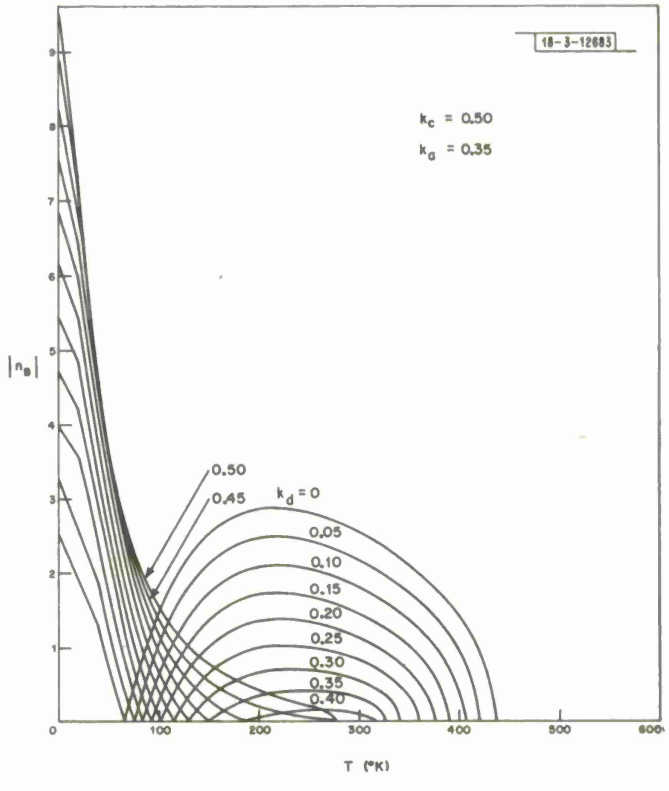

(h) For $k_a = 0.35$.

Fig. 24(a-h). Continued.

(a) For $k_a = 0$.

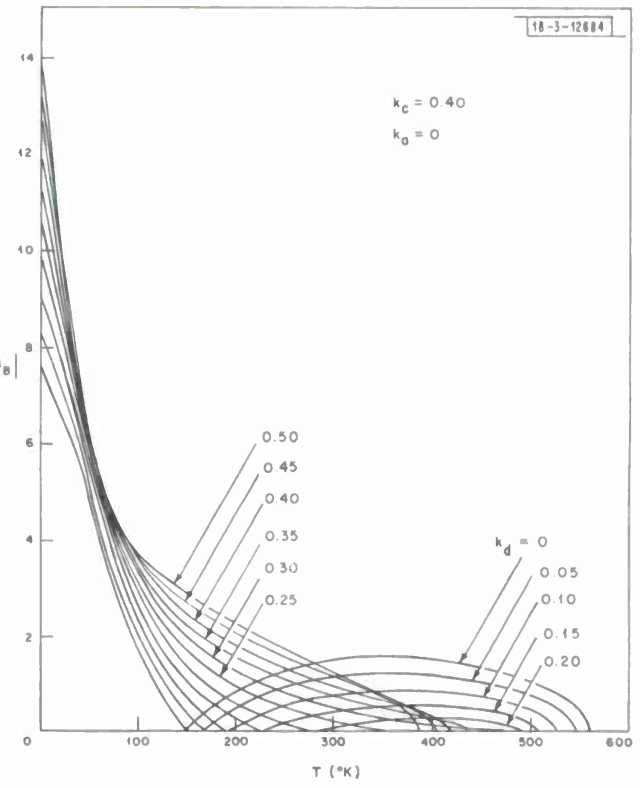

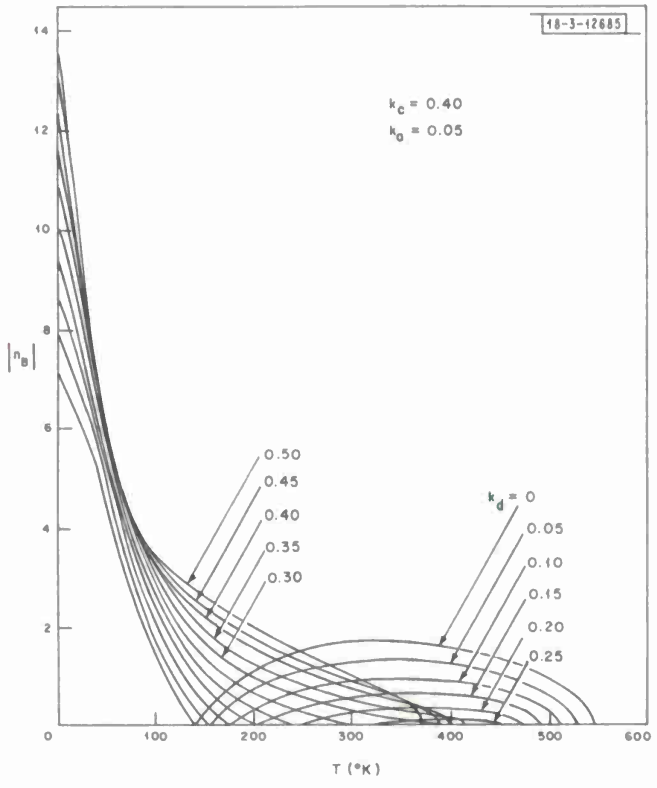

(b) For $k_a = 0.05$.

Fig. 25(a-h). Magnetic moment $|n_B|$ vs T for $k_c = 0.40$, $0 \leqslant k_d \leqslant 0.50$, k_a (as indicated).

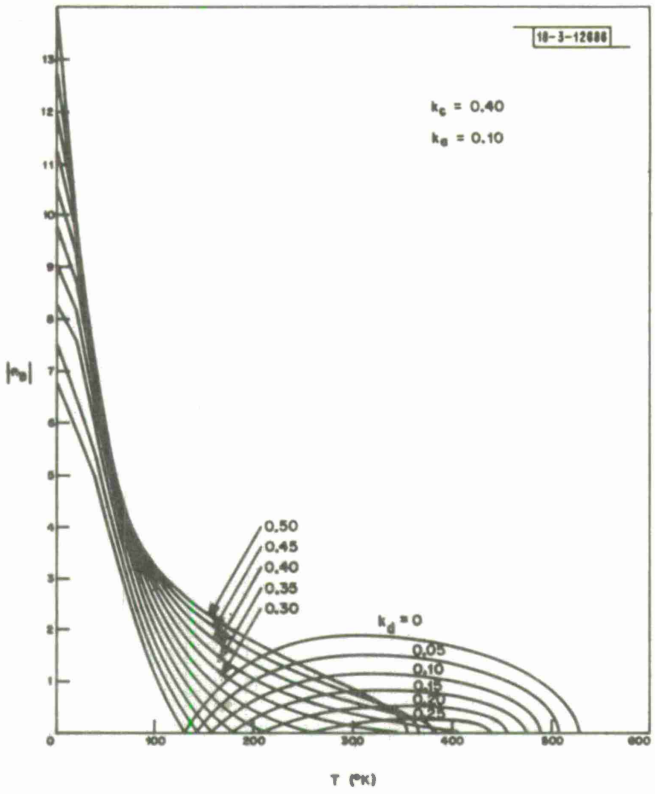

(c) For $k_a = 0.10$.

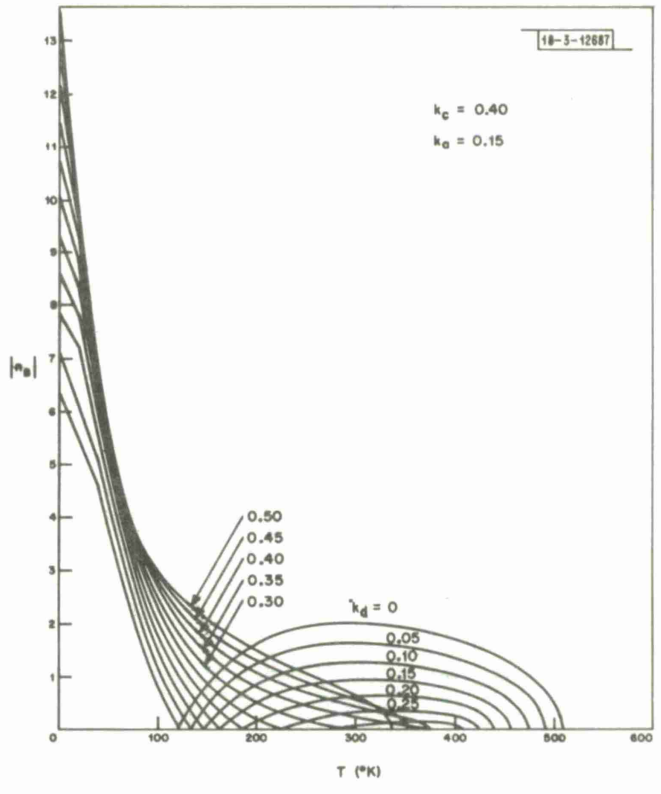

(d) For $k_a = 0.15$.

Fig. 25(a-h). Continued.

(e) For $k_a = 0.20$.

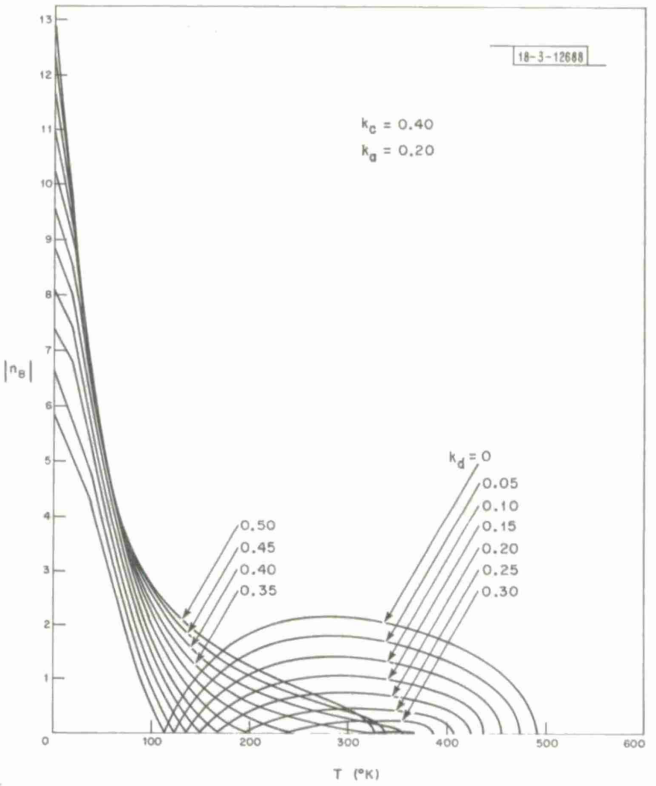

(f) For $k_a = 0.25$.

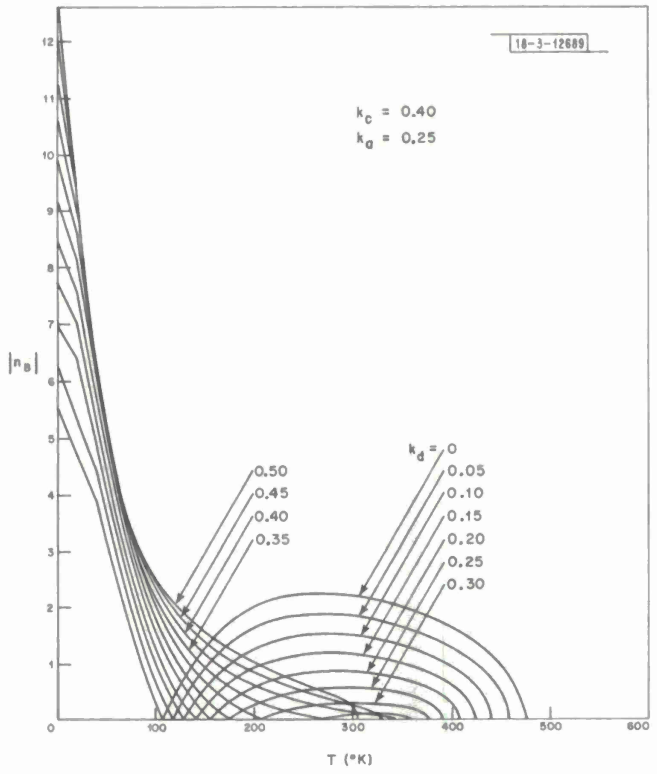

Fig. 25(a-h). Continued.

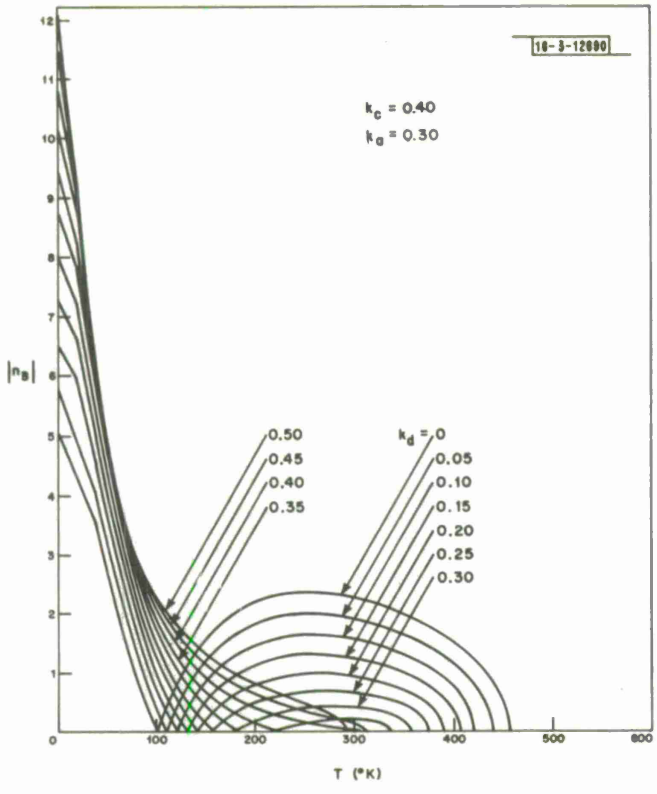

(g) For $k_a = 0.30$.

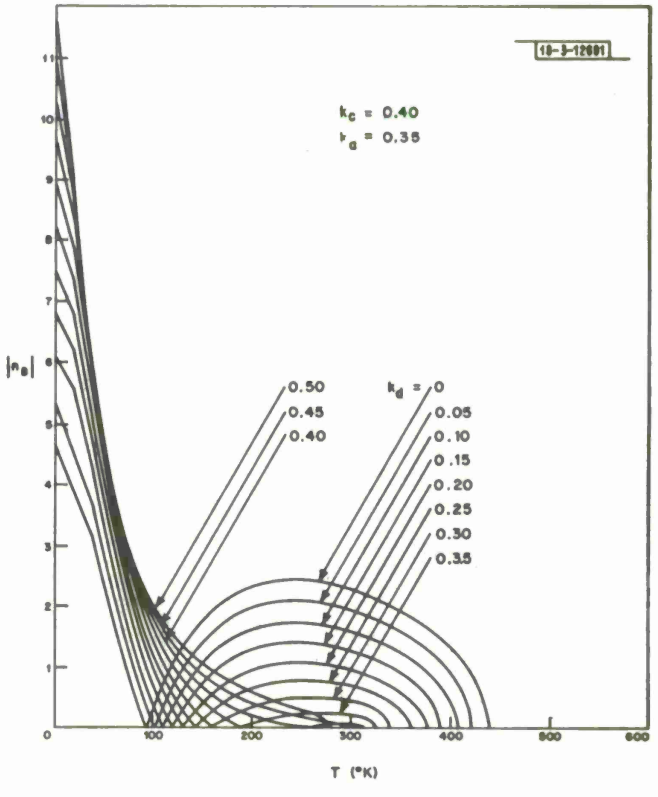

(h) For $k_a = 0.35$.

Fig. 25(a-h). Continued.

DOCUMENT CONTROL DATA – R&D

(Security classification of title, body of abstract and indexing annotation must be entered when the overall report is classified)

1. ORIGINATING ACTIVITY *(Corporate author)* Lincoln Laboratory, M.I.T.	2a. REPORT SECURITY CLASSIFICATION Unclassified 2b. GROUP None

3. REPORT TITLE

Magnetic Moment Versus Temperature Curves of Ferrimagnetic Garnet Materials

4. DESCRIPTIVE NOTES *(Type of report and inclusive dates)*

Technical Report

5. AUTHOR(S) *(Last name, first name, initial)*

Dionne, Gerald F.

6. REPORT DATE	7a. TOTAL NO. OF PAGES	7b. NO. OF REFS
9 September 1970	60	14

8a. CONTRACT OR GRANT NO. AF 19(628)-5167 b. PROJECT NO. 7X263304D215 c. d.	9a. ORIGINATOR'S REPORT NUMBER(S) TR 480 9b. OTHER REPORT NO(S) *(Any other numbers that may be assigned this report)* ESD-TR-70-150

10. AVAILABILITY/LIMITATION NOTICES

This document has been approved for public release and sale; its distribution is unlimited.

11. SUPPLEMENTARY NOTES	12. SPONSORING MILITARY ACTIVITY
None	Office of the Chief of Research and Development, Department of the Army

13. ABSTRACT

The molecular field coefficients employed in the Néel theory of ferrimagnetism have been determined as functions of the levels of diamagnetic ion substitution in the garnet family $\{Y_zGd_{3-z}\}\,[R_xFe_{2-x}]\,(Q_yFe_{3-y})O_{12}$, where R and Q represent diamagnetic octahedral and tetrahedral substitutions, respectively. The coefficients may be listed as

$$N_{dd} = -30.4(1 - 0.43x) \qquad N_{ad} = 97.0(1 - 0.125x - 0.127y)$$

$$N_{aa} = -65.0(1 - 0.42y) \qquad N_{cd} = 6.0$$

$$N_{cc} = 0 \qquad N_{ac} = -3.44 \text{ moles/cm}^3$$

With these coefficients the magnetic moment versus temperature curves of compositions ranging from $0 \leqslant x \leqslant 0.70$, $0 \leqslant y \leqslant 1.95$, and $0.40 \leqslant z \leqslant 1.00$ were computed and are presented in this report.

14. KEY WORDS

ferrimagnetic materials solid state physics garnets

Printed by
United States Air Force
L. G. Hanscom Field
Bedford, Massachusetts